NeuroImage 261 (2022) 119511

Contents lists available at ScienceDirect

NeuroImage

journal homepage: www.elsevier.com/locate/neuroimage

Covariance-based vs. correlation-based functional connectivity dissociates healthy aging from Alzheimer disease

Jeremy F. Strain[a,1], Matthew R. Brier[a,1], Aaron Tanenbaum[a], Brian A. Gordon[b,c,d], John E. McCarthy[e], Aylin Dincer[b], Daniel S. Marcus[b,c], Jasmeer P. Chhatwal[g], Neill R. Graff-Radford[h], Gregory S. Day[h], Christian la Fougère[i,j], Richard J. Perrin[a,c,f,k], Stephen Salloway[l], Peter R. Schofield[m,n], Igor Yakushev[o], Takeshi Ikeuchi[p], Jonathan Vöglein[q], John C. Morris[a,c], Tammie L.S. Benzinger[b,c], Randall J. Bateman[a,c,f], Beau M. Ances[a,b,f], Abraham Z. Snyder[a,b,*], For the Dominantly Inherited Alzheimer Network[1]

[a] Department of Neurology, Washington University in Saint Louis, St. Louis, MO 63110, USA
[b] Department of Radiology, Washington University in Saint Louis, Box 8225, 660 South Euclid Ave, St. Louis, MO 63110, USA
[c] Knight Alzheimer Disease Research Center, Washington University in St. Louis, St. Louis, MO 63110, USA
[d] Department of Psychological & Brain Sciences, Washington University, St. Louis, MO, USA
[e] Department of Mathematics and Statistics, Washington University, St. Louis, MO 63130, USA
[f] Hope Center for Neurological Disorders, Washington University in St. Louis, St. Louis, MO 63110, USA
[g] Martinos Center, Massachusetts General Hospital, 149 13th St Room 2662, Charlestown, MA 02129, USA
[h] Department of Neurology, Mayo Clinic Florida, 4500 San Pablo Road, Jacksonville, Fl 32224, USA
[i] Department of Nuclear Medicine and Clinical Molecular Imaging, Universityhospital Tübingen, Tübingen, Germany
[j] German Center for Neurodegenerative Diseases (DZNE) Tübingen, Germany
[k] Department of Pathology and Immunology, Washington University in St. Louis, St. Louis, MO 63110, USA
[l] Alpert Medical School of Brown University, 345 Blackstone Boulevard, Providence, RI 02906, USA
[m] Neuroscience Research Australia, Sydney, NSW 2131, Australia
[n] School of Medical Sciences, University of New South Wales, Sydney, NSW 2052, Australia
[o] Department of Nuclear Medicine, Klinikum Rechts der Isar, School of Medicine, Technical University of Munich, Ismaninger Str. 22, Munich 81675, Germany
[p] Department of Molecular Genetics, Brain Research Institute, Niigata University, Japan
[q] Department of Neurology, Ludwig-Maximilians-Universität Munich, Germany

ARTICLE INFO

Keywords:
Resting-state functional connectivity
Covariance
Aging
Late onset Alzheimer disease
Autosomal dominant Alzheimer disease

ABSTRACT

Prior studies of aging and Alzheimer disease have evaluated resting state functional connectivity (FC) using either seed-based correlation (SBC) or independent component analysis (ICA), with a focus on particular functional systems. SBC and ICA both are insensitive to differences in signal amplitude. At the same time, accumulating evidence indicates that the amplitude of spontaneous BOLD signal fluctuations is physiologically meaningful. We systematically compared covariance-based FC, which is sensitive to amplitude, vs. correlation-based FC, which is not, in affected individuals and controls drawn from two cohorts of participants including autosomal dominant Alzheimer disease (ADAD), late onset Alzheimer disease (LOAD), and age-matched controls. Functional connectivity was computed over 222 regions of interest and group differences were evaluated in terms of components projected onto a space of lower dimension. Our principal observations are: (1) Aging is associated with global loss of resting state fMRI signal amplitude that is approximately uniform across resting state networks. (2) Thus, covariance FC measures decrease with age whereas correlation FC is relatively preserved in healthy aging. (3) In contrast, symptomatic ADAD and LOAD both lead to loss of spontaneous activity amplitude as well as severely degraded correlation structure. These results demonstrate a double dissociation between age vs. Alzheimer disease and the amplitude vs. correlation structure of resting state BOLD signals. Modeling results suggest that the AD-associated loss of correlation structure is attributable to a relative increase in the fraction of locally restricted as opposed to widely shared variance.

* Corresponding author at: Department of Radiology, Washington University in Saint Louis, Box 8225, 660 South Euclid Ave, St. Louis, MO 63110, USA.
E-mail address: avi@npg.wustl.edu (A.Z. Snyder).
[1] These authors contributed equally to this work.

https://doi.org/10.1016/j.neuroimage.2022.119511.
Received 13 February 2022; Received in revised form 4 July 2022; Accepted 22 July 2022
Available online 30 July 2022.

1. Introduction

The literature on resting state fMRI functional connectivity (FC) in aging and Alzheimer disease (AD) is extensive[1]. The consensus view is that FC generally becomes weaker with advancing age, especially within the default mode network (DMN) (Spreng and Schacter 2012; Ferreira and Busatto 2013; Dennis and Thompson 2014; Sala-Llonch et al., 2015; Damoiseaux 2017). Similar findings have been reported in AD (Greicius et al., 2004; Mevel et al., 2011), i.e., prominent FC decreases especially within the DMN. Importantly, it is the DMN in which the characteristic distribution of neuropathology is most prominent in AD (amyloid beta (Aβ)/tau accumulation, atrophy) (Matthews et al., 2013; Sheline and Raichle 2013; Dennis and Thompson 2014; Forouzannezhad et al., 2019). Thus, it has been suggested that loss of FC in higher order functional systems, especially the DMN, may be more prominent in AD as compared to aging (Jones et al., 2011; Toepper 2017; Chhatwal et al., 2018; Lin et al., 2018). However, this inference is based on relatively few studies, which leaves open the question of whether the effects of healthy aging vs. AD are distinguishable strictly on the basis of FC.

Autosomal dominant AD (ADAD), an uncommon variant (~1% of all cases), defined by mutations in presenilin 1, presenilin 2, or amyloid precursor protein (APP) genes causes symptomatic disease in relatively young patients. Longitudinal studies of ADAD and late onset AD (LOAD) demonstrate similar pathology: Aβ plaques develop early (Bateman et al., 2012; Gordon et al., 2018; McDade et al., 2018) followed by tau accumulation, neurodegeneration, and finally cognitive decline (Bateman et al., 2012; Potter et al., 2013; Almkvist et al., 2017). Importantly, unlike LOAD, ADAD occurs in younger individuals. This difference offers a means of disentangling the effects of aging vs. pathology by studying AD in the absence of advanced age. Apart from age of onset, ADAD differs from LOAD in the distribution of neuropathology, specifically, greater subcortical atrophy and Aβ/tau deposition (Tentolouris-Piperas et al., 2017; Luckett et al., 2021). Notwithstanding this difference, the available evidence suggests that the FC manifestations of ADAD and LOAD are similar at comparable disease stages (Thomas et al., 2014; Chhatwal et al., 2018). However, a head-to-head comparison of FC in ADAD vs. LOAD, rigorously controlling for age, has not so far been reported.

Almost all prior work on FC in aging and AD has been cast in terms of either Pearson correlation, which is normalized, and therefore, invariant with respect to signal amplitude, e.g., (Damoiseaux 2017, Jalilianhasanpour et al. 2019), or ICA of time series normalized to unit variance, e.g., (Chhatwal et al. 2018, Forouzannezhad et al. 2019). These analyses remove from consideration systematic differences in the amplitude of spontaneous fMRI signal fluctuations. However, decreases in the amplitude of fMRI signal fluctuations have been reported in association with old age (Garrett et al., 2010; Grady and Garrett 2014; Vieira et al., 2020) as well as neurodegenerative disorders including AD (Luo et al., 2015; Mascali et al., 2015; Kazemifar et al., 2017; Marchitelli et al., 2018)[2]. These prior results suggest that insight can be gained by systematically comparing FC evaluated with vs. without signal normalization. This is most naturally done by comparing correlation-based FC to covariance-based FC, which is computationally identical except for omission of normalization (Varoquaux et al., 2010).

We adopt an extant data-driven approach based on whole-brain sampling of resting state BOLD fMRI signals from 222 regions of interest (ROIs) representing 12 resting state networks (RSNs; Fig. 1)(Seitzman et al., 2020). Representing FC data in a space of relatively low dimension using established techniques, e.g., principal component analysis, simplifies distinguishing between the effects of aging vs. AD and ADAD vs. LOAD. This is accomplished by assessing group differences in terms of components (Madsen et al., 2017). As will be shown below, almost all systems-level structure in 222 × 222 covariance and correlation matrices can be represented with only 30 components. A component-based approach to assessing group differences in FC also enables distinguishing between the effects of age vs. AD using straightforward regression.

We address three questions: (1) Do the effects of age and AD manifest differently in covariance- vs. correlation-base based FC? (2) what FC features distinguish AD (ADAD and LOAD) from healthy aging; (3) what FC differences, if any, distinguish ADAD from LOAD across clinical disease stages as measured by Clinical Dementia Rating (CDR^{TM}). To this end, we analyze covariance- and correlation-based FC evaluated globally over the entire brain.

2. Methods

2.1. Participants

ADAD participants (Table 1) were drawn from 14 international sites in the Dominantly Inherited Alzheimer Network (DIAN) observational study (www.dian-info.org). The DIAN recruits and follows families with disease-causing mutations in APP, PSEN1, and PSEN2 (Bateman et al., 2012). The DIAN cohort included mutation carriers (MC, $N = 123$) and corresponding non-carrier family members (NC; $N = 83$) who served as controls. Data utilized here were derived from the 11th semiannual data freeze.

Institutional review boards at Washington University in Saint Louis and participating institutions approved the protocols.

Data for LOAD participants was drawn from ongoing studies of aging and AD from the Charles F. and Joanne Knight Alzheimer Disease Research Center (ADRC) at Washington University School of Medicine (WUSM). All participants or their legal representative provided written informed consent. The institutional review board at Washington University in Saint Louis approved the protocols.

We analyzed data obtained in cognitively normal participants with ($N = 51$) and without ($N = 131$) biomarker evidence (amyloid PET) of preclinical LOAD and cognitively impaired participants with biomarker evidence of LOAD ($N = 50$). Demographics are listed in Table 1; 25 participants were excluded owing to excessive head motion.

2.2. Disease staging

Disease stage was defined by the Clinical Dementia Rating (CDR^{TM}) (Morris 1993). CDR scores of 0, 0.5, and ≥1 indicate, respectively, normal cognitive status, very mild dementia, and mild to moderate dementia. Amyloid (Aβ) positivity was defined by either [^{11}C]Pittsburgh compound B (PiB)(Klunk et al., 2004) or [^{18}F]florbetapir PET (Wong et al., 2010). Aβ positivity was defined, for PiB, as mean cortical binding potential (MCBP) ≥ 0.18 (Su et al., 2013) and, for florbetapir, a standardized uptake value ratio (SUVR) ≥1.2 (Mishra et al., 2017).

2.3. Imaging acquisition

LOAD participants were scanned at WUSM. Imaging of ADAD participants was conducted at their respective DIAN sites using local scanners. To increase the compatibility between DIAN and WUSM cohorts, we analyzed only data collected on Siemens 3T scanners (Erlangen, Germany). During resting state fMRI scans, participants were instructed to maintain visual fixation on a crosshair. fMRI runs were approximately

[1] As of October 21, 2021, a PubMed search on "resting state fMRI AND aging" returned 1377 hits of which 61 were reviews. "Resting state fMRI AND Alzheimer disease" returned 1098 hits of which 89 were reviews.

[2] The amplitude of spontaneous fMRI signal fluctuations has been variably evaluated as the temporal standard deviation (SD_{BOLD}) Garrett et al., (2010). "Blood oxygen level-dependent signal variability is more than just noise." J Neurosci **30**(14): 4914–4921. or as root mean squared power summed over a defined spectral range (ALFF) Zuo et al., (2010).. "The oscillating brain: complex and reliable." Neuroimage **49**(2): 1432–1445. The algebraic distinction between these measures is negligible.

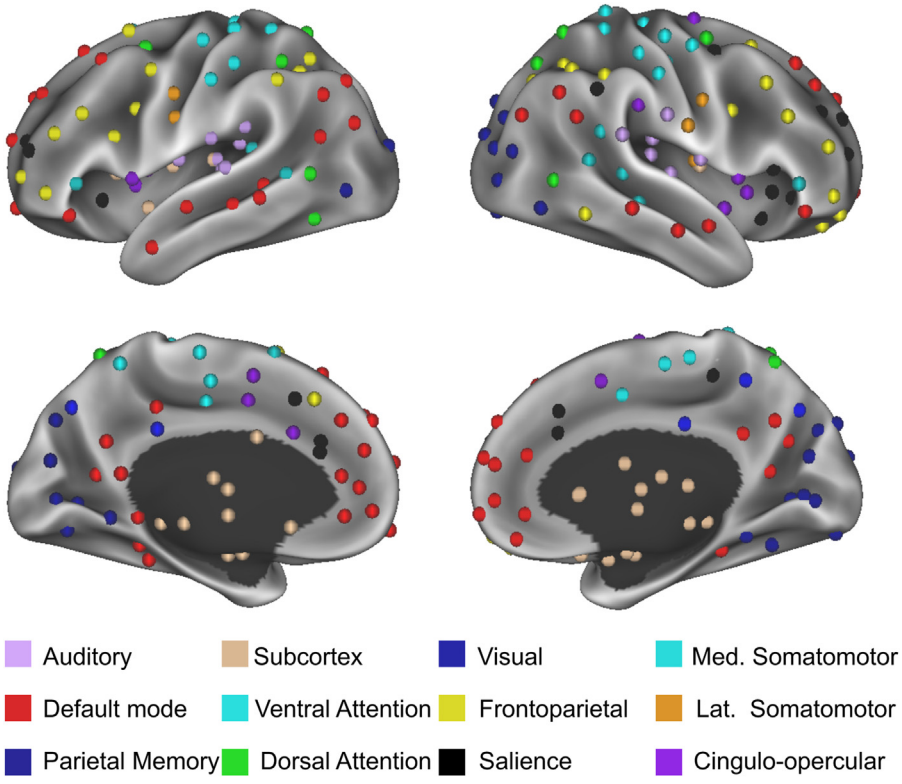

Fig. 1. Regions of Interest. Centers of the 222 regions of interest (ROI) used in this work are projected onto an average anatomical surface (Seitzman et al., 2020). Cortical and subcortical ROIs are spheres, 10mm and 8mm in diameter, respectively. Color indicates resting state network membership.

Table 1
Participant demographics. Total number fMRI frames (volumes) are summed across all runs acquired in each participant.

				N	M	F	Agemean	AgeSD	Total Frames	PercentCensored
WUSM cohort	LOAD Aβ-		Control	131	41	90	66.0	6.5	164	14.4
	LOAD		CDR 0	51	20	31	74.8	6.6	164	13.9
	Aβ+		CDR 0.5	39	21	18	69.0	5.0	164	14.4
			CDR ≥ 1	11	6	5	65.2	7.0	164	20.1
DIAN cohort	Mutation-	Aβ-	Control	83	34	49	39.8	11.3	195	18.2
	Mutation+	Aβ-	CDR 0	40	21	19	31.1	8.6	183	17.6
		Aβ+	CDR 0	31	15	16	36.8	6.7	177	16.4
			CDR 0.5	33	13	20	46.8	9.2	212	15.6
			CDR ≥ 1	19	9	10	50.2	8.6	169	18.5

6 min in duration. "Pre-scan normalize" was enabled to minimize gain field inhomogeneities attributable proximity to the receiver coils. Two resting state fMRI runs were acquired in the WUSM cohort. The number of acquired runs in the DIAN cohort varied between 1 and 3. Additional details concerning sequences and quantity of data is provided in Supplemental Table S1.

2.4. Initial FC preprocessing

FC pre-processing generally followed previously described methods (Laumann et al., 2017; Gratton et al., 2019) implemented in the 4dfp suite of tools (http://4dfp.readthedocs.io). This included slice timing correction and correction of odd versus even slice intensity differences attributable to interleaved acquisition (see Supplemental Materials in Hacker et al. (2013)). Head motion was corrected within and across runs. Intensity inhomogeneity was corrected using the FAST module in FSL (Zhang et al., 2001) followed by intensity normalization (one multiplicative scalar applied to all voxels and volumes) to obtain a whole brain mode value of 1000. Echoplanar imaging (EPI) distortion due to magnetization inhomogeneity was corrected using the mean field map method of Gholipour et al. (2008). For the DIAN cohort, initial atlas transformation was computed by affine registration of the functional data to an atlas-representative template via the MP-RAGE (EPI_{mean} → MP-RAGE → template). The final atlas transformation was performed after denoising (see below). The WUSM data included a T2-weighted image that was inserted in the transform composition chain (EPI_{mean} → T2w → MP-RAGE → template). Volumetric time series were resampled in $(3mm)^3$ atlas space in a single step combining head motion correction, distortion correction, and atlas transformation. Frames corrupted by excessive head motion were identified on the basis of both DVARS (frame-to-frame signal change over the entire brain); and frame displacement (FD) measures (Power et al., 2012). The DVARS censoring criterion was individually set to accommodate baseline shifts (see Supporting Information in White et al. (2020); the FD censoring criterion was 0.4mm. Frames were censored if either criterion was exceeded. Censoring statistics are reported in Table 1. The time series were band-pass filtered to retain frequencies between 0.005 Hz and 0.1Hz. Censored frames were approximated by linear interpolation for purposes of band-pass filtering but excluded from all subsequent steps.

2.5. Denoising

Denoising was accomplished using a CompCor-like strategy (Behzadi et al., 2007). As previously described Raut et al. (2019), nuisance regressors were derived from three compartments (white matter, ventricles, and extra-axial space) and were then dimensionality-reduced

to create a matrix for singular value decomposition (SVD). White matter and ventricular masks were segmented in each participant using FreeSurfer (Fischl 2012) and spatially resampled in register with FC data. The final set of nuisance regressors also included the six parameters derived from rigid body head-motion correction, the global signal (GS) averaged over the (FreeSurfer-segmented) brain, and the GS temporal derivative. Appendix D shows that omitting regression of the global signal minimally impacts the present results. As a final preprocessing step, the volumetric time series were non-linearly warped (via each participant's MP-RAGE) to Montreal Neurological Institute (MNI) 152 space ($(3mm)^3$ voxels) using FNIRT (Andersson et al., 2010; Jenkinson et al., 2012).

2.6. FC computation

Pre-processed fMRI time series were extracted from 222 regions of interest (ROIs) representing 12 previously defined RSNs (Fig. 1) (Seitzman et al., 2020). This set of ROIs provides dense coverage of the cerebral cortex and subcortical structures. ROIs in areas of fMRI signal drop out (Ojemann et al., 1997) were excluded. The cerebellum was excluded owing to inadequate coverage of this structure in some ADAD participants; given the limited role of the cerebellum in AD we elected to forego including this region instead of excluding participants. FC was conventionally evaluated in terms of Pearson correlation as well as covariance, which is simply un-normalized correlation. Thus, covariance retains sensitivity to signal amplitude whereas correlation does not. Algebraic details are provided in Appendix A. Parallel covariance/correlation analysis constitutes a major feature of the present work.

Evaluating covariance rather than correlation requires minimizing the impact of artifactual differences in depth of signal modulation unrelated to physiology. In addition to enabling "pre-scan normalize" during fMRI acquisition (see above), residual gain field inhomogeneities were reduced using the FAST module in FSL (Zhang et al., 2001). Further, all fMRI data were intensity normalized (multiplication by a single scalar over all brain voxels and volumes) to obtain a consistent mode value of 1000 in all participants. Thus, a covariance value of 10 corresponds to 1% rms fMRI signal modulation.

2.7. Dimensionality reduction and derivation of fixed bases for covariance and correlation analyses

Sections 2.7 and 2.8 recapitulate algebra recently described in a different context (Snyder et al., 2022). The fixed basis on which all susbequent analyses of covariance FC depend was obtained by principal component analysis (PCA) (Liang et al., 2002) applied to the mean covariance matrix, $\bar{C}_{CONT}$, obtained in the combined WUSM + DIAN control participants. Diagonalization of $\bar{C}_{CONT}$ yields

$$\bar{C}_{CONT} = W \Lambda_{CONT} W^T \tag{1}$$

where the columns of W contain the eigenvectors of $\bar{C}_{CONT}$ and Λ_{CONT} is a diagonal matrix of eigenvalues. Dimensionality reduction was achieved by taking the first 30 eigenvectors of $\bar{C}_{CONT}$ as a fixed basis on which to project all covariance evaluations. Thus,

$$\hat{C}_{CONT} = \hat{W} \hat{\Lambda}_{CONT} \hat{W}^T \tag{2}$$

is the projection of $\bar{C}_{CONT}$ onto the covariance FC basis, $\hat{W}$. In the present data, the first 30 eigenvectors retained a large fraction (60.4%) of the total variance in $\bar{C}_{CONT}$. Projection of participant i's fMRI data (X_i, not necessarily a control) onto the fixed covariance basis was computed as $\hat{Y}_i = \hat{W}^T X_i$. The covariance matrix of $\hat{Y}_i$ is

$$\left(1/L_i\right) \hat{Y}_i \hat{Y}_i^T \tag{3}$$

where L_i is number of retained frames following frame censoring. We *define* the diagonal entries of this matrix, $\hat{\Lambda}_i$, as the of 30 covariance components in participant i and *define* $\hat{C}_i \equiv \hat{W} \hat{\Lambda}_i \hat{W}^T$ as the projection of participant i's covariance structure onto the fixed basis. The algebraic rationale for these definitions is given in Appendix A. Importantly, because $\hat{W}$ is fixed, $\hat{\Lambda}_i$ (a 30×30 diagonal matrix) and $\hat{C}_i$ (also a 30×30 diagonal matrix) are informationally equivalent. Moreover, $\{\hat{\Lambda}_i\}$, the covariance components corresponding to any subgroup of participants, can be subjected to algebraic operations, e.g., averaging over participant subgroups and regression operations. For notational simplicity, we define $\Psi_i \equiv \mathrm{diag}(\hat{\Lambda}_i)$ as the 30 covariance components in participant i reshaped as a 1×30 row vector.

Correlation FC analyses were conducted independently and in parallel to covariance FC analyses. The associated algebraic quantites are denoted in lower case symbols. Thus, for example, the correlation FC basis set, $\hat{w}$, was defined as the first 30 eigenvectors of the mean control correlation matrix, $\bar{r}_{CONT}$. The 30 retained correlation components accounted for 54.9% of total variance. In parallel to Ψ_i, $\psi_i \equiv \mathrm{diag}(\hat{\lambda}_i)$ is the row vector of 30 correlation components in participant i. All symbols used in the presentation of results are listed in Table 2. Parallel covariance/correlation analysis is implicit in format of Table 2. Additional algebraic details are discussed in Appendix A.

2.8. Covariance:correlation global scalar proportionality

Inspection of $\hat{C}_{\mathrm{CONT}}$ and $\hat{r}_{CONT}$ suggested that these forms exhibit strikingly similar "matrix topographies" (see Results), i.e., differ, to good approximation, only by a global scalar factor proportional to the amplitude of BOLD signal fluctuations. Hence, the model, $\hat{C}_{CONT} \approx \upsilon_{CONT} \hat{r}_{CONT}$, where υ_{CONT} is a scalar. We refer to this scalar quantity as the global covariance:correlation proportionality constant. Details concerning estimation of υ are given in Appendix A. As υ is defined in controls as well as participant subgroups, this measure provides a quantitative index of the dissociation between the amplitude vs. the correlation structure of spontaneous BOLD signals.

Table 2 lists the variables used in the presentation of results. Asterisk subscripts stand for any subgroup, e.g., LOAD CDR1+. Note that the bases, $\hat{W}$ and $\hat{w}$, are fixed (therefore, represented without subscripts).

Table 2
Symbols referring to measured quantities in the presentation of results. Asterisks stand for any subgroup, e.g., LOAD CDR1 as well as control participants. The dimensionality of regression coefficients (:) depends on model details.

	covariance	correlation	dimension
full dimensionality FC matrix	$\boldsymbol{C}_*$	$\boldsymbol{r}_*$	222×222
eigenvectors of FC matrix	$\boldsymbol{\Lambda}_*$	$\boldsymbol{\lambda}_*$	222×222
basis derived by PCA of control group FC matrices	$\hat{\boldsymbol{W}}$	$\hat{\boldsymbol{w}}$	222×30
dimensionality reduced FC matrix	$\hat{\boldsymbol{C}}_*$	$\hat{\boldsymbol{r}}_*$	222×222
component values derived by projection on basis	$\boldsymbol{\Psi}_*$	$\boldsymbol{\psi}_*$	1×30
regression coefficients	B^*	$\boldsymbol{\beta}^*$	$30 \times$:
global $\hat{\boldsymbol{C}}_*$: $\hat{\boldsymbol{r}}_*$ proportionality constant	$\boldsymbol{\upsilon}_*$		scalar
fraction of variance accounted for by the $\hat{\boldsymbol{C}}_*$: $\hat{\boldsymbol{r}}_*$ model	$\boldsymbol{\eta}_*$		scalar

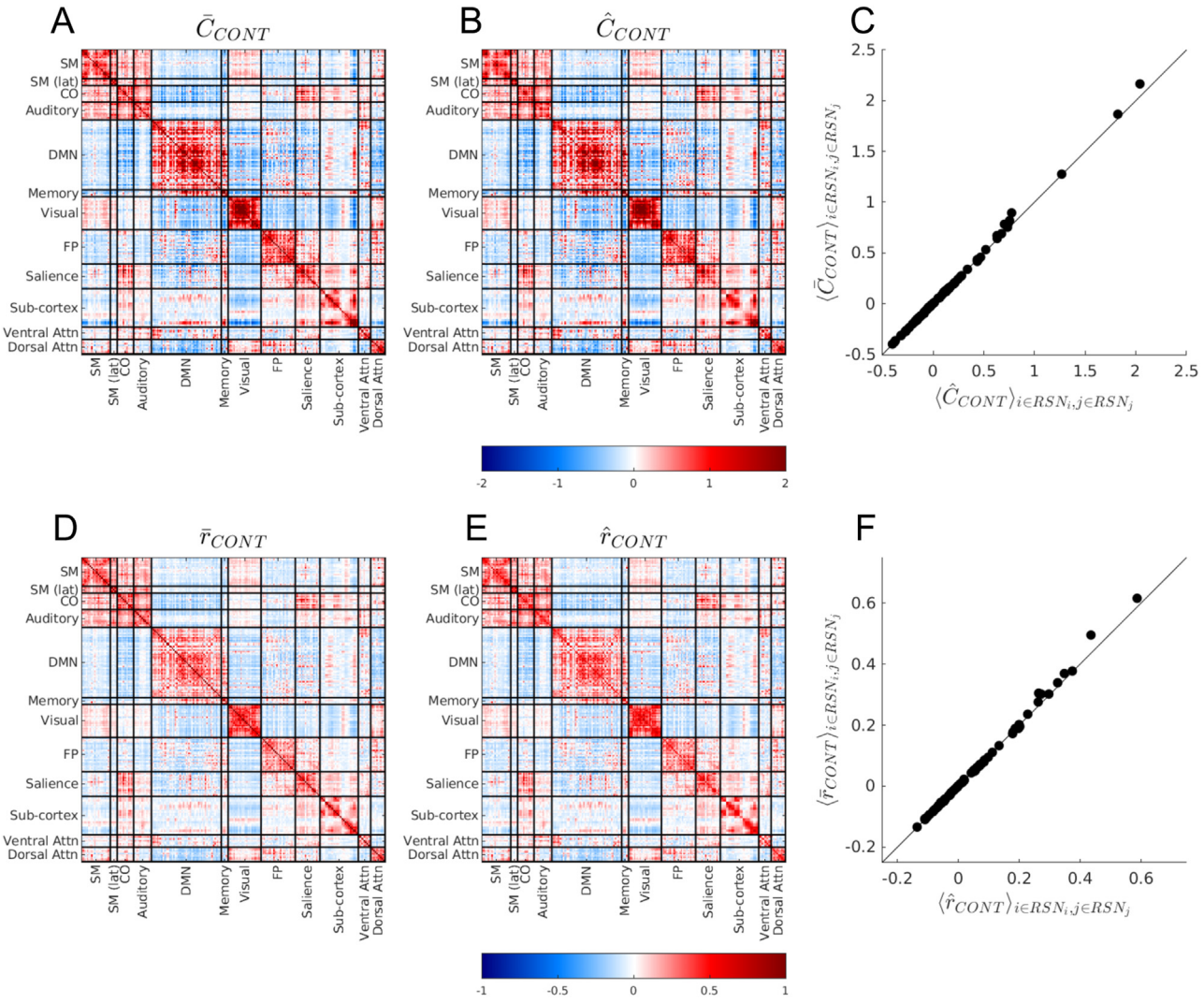

Fig. 2. Dimensionality reduction preserves resting state network-dependent features of covariance and correlation matrices. Panel A shows the covariance matrix mean in the control subjects ($\bar{\mathbf{C}}_{\mathbf{CONT}}$) before dimensionality reduction. The key feature of this matrix is consistently positive covariance within network (diagonal blocks) and between network covariance of either sign (off diagonal blocks). Panel B shows the dimensionality reduced covariance matrix mean in control subjects ($\hat{\mathbf{C}}_{\mathbf{CONT}}$). It is evident that $\bar{\mathbf{C}}_{\mathbf{CONT}}$ and $\hat{\mathbf{C}}_{\mathbf{CONT}}$ are remarkably similar. Quantitatively minor, within block differences between $\bar{\mathbf{C}}_{\mathbf{CONT}}$ vs. $\hat{\mathbf{C}}_{\mathbf{CONT}}$ could represent sub-network structure outside the fixed basis but could also arise from sampling error. To demonstrate that dimensionality reduction minimally impacts network structure, the mean within-block covariance values in $\bar{\mathbf{C}}_{\mathbf{CONT}}$ and $\hat{\mathbf{C}}_{\mathbf{CONT}}$ are shown as a scatter plot in panel C; these values closely approximate the line of identity. Panels D-F show parallel results for the corresponding correlation matrices, before ($\bar{\mathbf{r}}_{\mathbf{CONT}}$) and after ($\hat{\mathbf{r}}_{\mathbf{CONT}}$) dimensionality reduction. Note different covariance vs. correlation scales. These scale differences reflect crucial features of the present data, as detailed in subsequent figures. Network label abbreviations: SM – sensorimotor, SM (lat) – lateral sensorimotor, DMN – default mode network, FP – frontoparietal, Attn – attention.

2.9. Estimation of the effects of age and AD using linear regression

The effects of age and cohort (WUSM vs. DIAN) on FC components was estimated in the control participants using the *regress* function in MATLAB 2020b. For each component (j =1, 2, …, 30), Ψ_i or ψ_i were entered into the regression model with intercept (column of 1's), participant age, and cohort (0 or 1 representing ADRC or DIAN) as regressors. For covariance FC, regression returned 30 component-specific constants: change/year (B_j^{Age}), intercept (component estimate at age 0; B_j^{Int}), and a term accounting for cohort (WUSM vs. DIAN; B_j^{Cohort}). The $\{B_j^{Age}\}$ were used construct FC covariance matrices representing the effect of age, controlling for cohort. Parallel regression operations on correlation FC returned β_j^{Age}, β_j^{Int}, β_j^{Cohort}, $j = 1, 2, \ldots 30$. Next, the regression model was applied to all participants to reconstruct group-level FC matrices at selected CDR stages (0, 0.5, 1+) from which the effects of age and cohort have been removed by regression. Thus, (corrected Ψ_{ij}) = (uncorrected Ψ_{ij}) $-B_j^{Age}(Age)_i - B_j^{Cohort}(Cohort)_i$. The corrected component results were averaged over participants to generate group-level component vectors, e.g., $\bar{\Psi}_*$ for covariance FC, where the overbar denotes averaging over participants and the asterisk represents a particular subgroup, e.g., LOAD CDR 1+.

2.10. Statistical significance testing

Whole-brain, group-level contrasts are represented as the L1-norm of component differences $|\Delta\bar{\Psi}_*|$ and $|\Delta\bar{\psi}_*|$, where the asterisk represents a particular group contrast, e.g., LOAD CDR 1+ vs. controls. The rationale underlying this formulation is that, to the extent that all participants share the identical FC eigenstructure (see Appendix A), $|\Delta\bar{\Psi}_*|$ is equivalent to the sum of over components of power differences. The

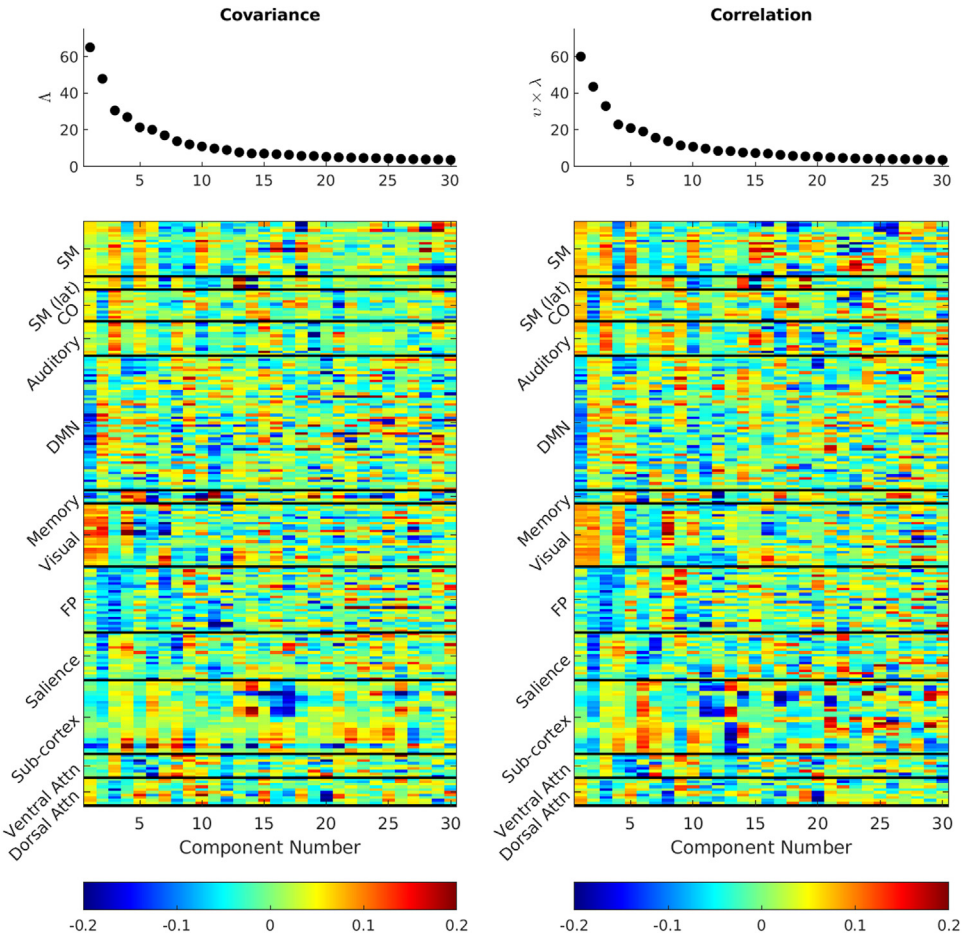

Fig. 3. Principal component analysis of ($\hat{\mathbf{C}}_{\mathbf{CONT}}$) and correlation ($\hat{\mathbf{r}}_{\mathbf{CONT}}$) matrices obtained in the control participants. Scree plots are shown above corresponding eigenvectors. The correlation eigenvectors have been multiplied by the scalar constant ($\upsilon_{\mathbf{CONT}} = 2.98$) that minimizes error in the proportionality model, $\langle \hat{\mathbf{C}}_{\mathbf{CONT}} \rangle_{\mathbf{k}} = \upsilon_{\mathbf{CONT}} \langle \hat{\mathbf{r}}_{\mathbf{CONT}} \rangle_{\mathbf{k}}$. The first few eigenvectors exhibit clustered, large loadings within resting state networks, e.g., the DMN. Network structure becomes fragmented at higher eigenvector indices in both the covariance and correlation representations of FC.

significance of group-level contrasts was assessed by comparing the true value of $|\Delta\bar{\Psi}_*|$ (or $|\Delta\bar{\psi}_*|$) against a null generated by permutation resampling over participants.

3. Results

3.1. Dimensionality reduction

Fig. 2 shows the mean control covariance and correlation matrices before ($\bar{C}_{CONT}$, $\bar{r}_{CONT}$) and after ($\hat{C}_{CONT}$, $\hat{r}_{CONT}$) projection onto their respective fixed bases. The block structure of these matrices, before and after projection onto the fixed bases, replicates established findings reported in multiple rs-fMRI studies (Laumann et al., 2015; Gotts et al., 2020; Seitzman et al., 2020). It is visually evident that the major features of $\bar{C}_{CONT}$ are preserved in $\hat{C}_{CONT}$ and similarly for $\bar{r}_{CONT}$ vs. $\hat{r}_{CONT}$. Although the projection accounts for only 60.4% of total variance in $\bar{C}_{CONT}$, the squared Pearson correlation between the block averages before vs. after dimensionality reduction, i.e., $\langle \bar{C}_{CONT} \rangle_k$ and $\langle \hat{C}_{CONT} \rangle_k$ (see Appendix A), is 0.998 (Fig. 2C). Similarly, the squared Pearson correlation between $\langle \bar{r}_{CONT} \rangle_k$ and $\langle \hat{r}_{CONT} \rangle_k$ is 0.997 (Fig. 2F). These results demonstrate that dimensionality reduction preserves the network structure of both covariance and correlation FC.

Anatomical topography of covariance and correlation bases

Fig. 3 shows scree plots and ROI weights for each of the 30 covariance ($\hat{W}$) and correlation ($\hat{w}$) basis vectors derived by PCA of the combined WUSM + DIAN control participants. Both $\hat{W}$ and $\hat{w}$ are structured according to major functional systems. Thus, for example, the first component of both $\hat{W}$ and $\hat{w}$ is dominated by oppositely signed DMN vs. visual system (VIS) weights. The second component includes oppositely signed cingulo-opercular + salience + fronto-parietal weights vs. VIS + DMN weights. Higher components exhibit progressively less RSN structure. Fragmentation of RSN-related structure, coupled with asymptotically small eigenvalues as component indices approach 30, implies that dimensionality reduction largely preserves the functional organization of BOLD fMRI time series, reinforcing the result illustrated in Fig. 2. Similarity of the covariance vs. correlation bases is addressed also in Fig. S4, which shows $\hat{W}^T\hat{w}$, the 30×30 matrix of inner products. The largely diagonal structure of $\hat{W}^T\hat{w}$ demonstrates substantial similarity of the bases derived by PCA of $\hat{C}_{CONT}$ and $\hat{r}_{CONT}$.

3.2. Covariance:correlation global scalar proportionality

Fig. 4 shows the covariance and correlation matrices obtained in the combined WUSM + DIAN control groups. It is evident that these matrices exhibit strikingly similar "matrix topographies". The global covariance:correlation ration in the controls is 2.98 (υ_{CONT}; see Appendix Eq. (8)). The proportion of model-consistent variance (η^2_{CONT}) is 0.94. Panel C shows the difference, $\hat{C}_{CONT} - \upsilon_{CONT}\hat{r}_{CONT}$, i.e., focal deviations from global proportionality. Such deviations include somewhat greater covariance:correlation ratios in parts of the DMN and somewhat lesser ratios in somatomotor cortex. Although these deviations are potentially of physiological interest, they are quantitatively minor (6% of explained variance). Taking into consideration this low proportion of explained variance, we defer further analysis of focal deviations from global covariance:correlation proportionality to future work.

Table 3 lists υ_* and η^2_* obtained in the ADRC and DIAN participants stratified by CDR. There are two noteworthy findings. First, the global covariance:correlation ratio systematically decreases with disease pro-

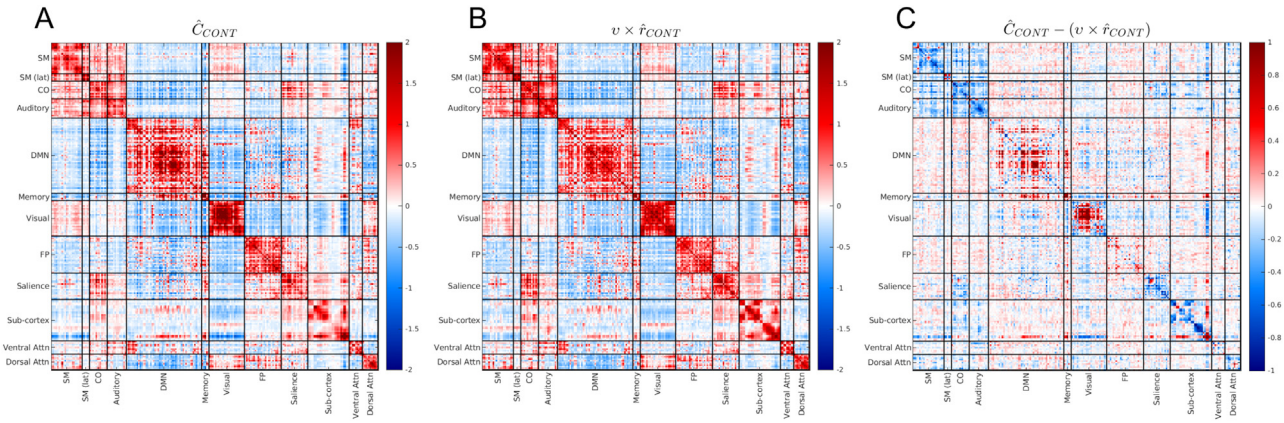

Fig. 4. Blockwise scalar proportionality between covariance and correlation matrices in the control population. Panel A shows $\hat{\mathbf{C}}_{\mathbf{CONT}}$. Panel B shows $v_{\mathbf{CONT}}\hat{\mathbf{r}}_{\mathbf{CONT}}$. Panel C shows the difference, $\hat{\mathbf{C}}_{\mathbf{CONT}} - v_{\mathbf{CONT}}\hat{\mathbf{r}}_{\mathbf{CONT}}$, i.e., focal deviations from block-wise scalar proportionality. These deviations account for only 6% of total variance ($\eta^2_{\mathbf{CONT}} = 0.94$). Note scale change in panel C.

Table 3
Global covariance:correlation ratios (v_*) and fraction of explained variance (η^2_*) for ADRC and DIAN participants stratified by CDR.

				v_*	η^2_*
WUSM cohort	LOAD Aβ-		Control	2.90	0.966
	LOAD		CDR 0	2.84	0.967
	Aβ+		CDR 0.5	2.82	0.965
			CDR ≥ 1	2.09	0.965
DIAN cohort	Mutation-	Aβ-	Control	2.41	0.962
	Mutation+	Aβ-	CDR 0	3.14	0.969
		Aβ+	CDR 0	2.48	0.955
			CDR 0.5	1.99	0.961
			CDR ≥ 1	1.28	0.973

gression, both in the LOAD and ADAD cohorts, albeit more steeply in the ADAD cohort. Second, variance explained by the proportionality model is remarkably robust ($\eta^2_* \approx 0.96$ in all groups) and not affected by disease progression.

3.3. Effect of age in the controls

Fig. 5 represents the effects age in the combined WUSM + DIAN controls. Covariance FC and correlation FC are shown in Panels A and B, respectively. The effect of age was estimated by regression of covariance components (Ψ_{ij}) on age, with cohort (ADRC or ADAD) as a regressor of no interest. This regression yielded coefficients, B_j^{Age}, $j = 1, 2, \ldots 30$, in units of covariance component change per year. The displayed covariance age effect matrix is $\hat{W}[diag B^{Age}]\hat{W}^T$. Aging leads to weaker within-RSN covariance (blue diagonal blocks) as well as weaker cross-RSN negative covariance (primarily red off-diagonal blocks). The effect of age on correlation FC is qualitatively similar but quantitatively much weaker. The displayed matrix is $v_{CONT}\hat{w}[diag\beta^{Age}]\hat{w}^T$. Panel C plots B_j^{Age} vs. B_j^{Int}, i.e., change per year in covariance component j vs. component j value extrapolated to age 0. The slope of the fitted line is 1.69% loss per year. The relatively good fit (Pearson correlation = -0.985; $p < 10^{-6}$) indicates that all covariance components exhibit approximately the same proportional loss relative to the starting value. Panel D shows the parallel result for correlation components, scaled by v_{CONT}. The model fit is less good but still quite strong (Pearson correlation = -0.856). Crucially, the fitted line (slope = -0.48%) indicates that correlation FC loss per year is numerically much less than covariance FC loss (-0.48% vs. -1.69%). This difference between the effects of age on covariance vs. correlation FC is discussed theoretically in Appendix B.

3.4. Effects of AD represented as dimensionality-reduced, covariance and correlation difference matrices

Fig. 6 shows dimensionally reduced, covariance difference matrices relative to controls at successive clinical disease stages of LOAD (panels B - D) and ADAD (panels F - H). The effects of age and cohort have been removed by regression. Corresponding, undifferenced matrices are shown in Fig. S1. Panel A (effect of age) is reproduced from Fig. 5A for comparison. It is visually evident that the impact of AD on covariance FC is minimal prior to CDR stage 1. Weak, non-significant, sign-inverted effects are present in older, Aβ+, CDR 0 LOAD participants (panel B) and younger, mutation-positive, Aβ- ADAD participants (panel E). Note strikingly similar "matrix topographies" (e.g., detailed patterning in the sub-cortical diagonal block), with or without sign inversion, in all matrices.

Fig. 7 shows dimensionally reduced, correlation difference matrices parallel to the results shown in Fig. 6. As in the covariance FC results, inspection suggest that the impact of AD on correlation FC is minimal prior to CDR stage 1. This is verified in Table 4, which reports significance tests of group-level contrasts in covariance FC and correlation FC. Significance levels were consistently greater for correlation as opposed to covariance FC.

3.5. Differential impact of LOAD and ADAD on covariance and correlation components

Fig. 8 addresses the question of whether either variant of AD differentially impacts particular covariance or correlation components. Each panel reports a group-level analysis of the 30 component values corresponding to the fixed basis ($\Delta\bar{\Psi}_j$ or $\Delta\bar{\psi}_j$), averaged over selected participant groups.

Similar effects are evident in panels A and B, which show covariance component differences (CDR 1+ minus control) for LOAD and ADAD. Slopes of the fitted lines (−0.564 and −0.436) indicate that, at CDR 1+ (mild dementia), component values are, on average, attenuated by a factor of approximately 1/2 relative to controls. The line fits are somewhat less tight than in Fig. 5C, consistent with the possibility that AD differentially impacts certain covariance components. Panel C plots $\Delta\bar{\Psi}_j$ for ADAD vs. $\Delta\bar{\Psi}_j$ for LOAD to address the question of differential component specificity in ADAD vs. LOAD at CDR 1+. The relatively tight correlation (Pearson correlation = 0.944, $p < 10^{-6}$) suggests that ADAD and LOAD comparably affect covariance FC components. In other words, there is no evidence of differential focality in the effects of ADAD vs. LOAD on whole-brain FC.

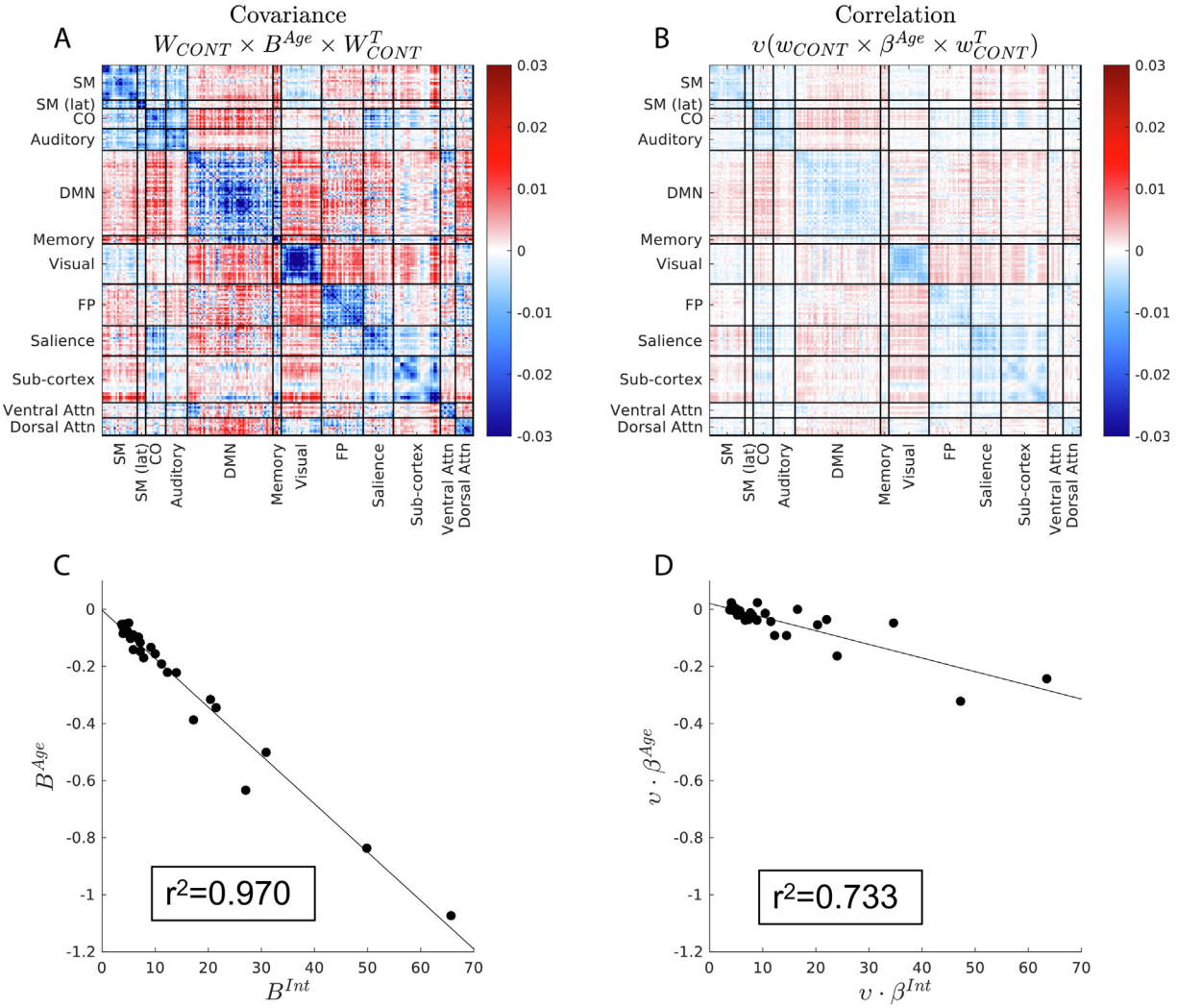

Fig. 5. Effect of age in the control participants. Panel A shows the effects of age on covariance FC, evaluated as $\hat{\mathbf{W}}[\mathbf{diag}\mathrm{B}^{\mathbf{age}}]\hat{\mathbf{W}}^{\mathbf{T}}$. Panel B shows the corresponding correlation FC result, evaluated as $\upsilon_{\mathbf{CONT}}\hat{\mathbf{w}}[\mathbf{diag}\boldsymbol{\beta}^{\mathbf{age}}]\hat{\mathbf{w}}^{\mathbf{T}}$. The scales are identical. The effect of cohort has been removed by regression. Panel C shows $\mathrm{B}_{\mathbf{j}}^{\mathbf{Age}}$ plotted against $\mathrm{B}_{\mathbf{j}}^{\mathbf{Int}}$, the intercept term, i.e., the value of covariance component **j** extrapolated to age 0. Note approximately uniform proportional effect of age across components (r^2=0.970). The slope the fitted line indicates -1.69% covariance component change per year relative to value at age 0. Panel D shows $\upsilon_{\mathbf{CONT}}\boldsymbol{\beta}_{\mathbf{j}}^{\mathbf{Age}}$ plotted against $\upsilon_{\mathbf{CONT}}\boldsymbol{\beta}_{\mathbf{j}}^{\mathbf{Int}}$, i.e., correlation result parallel to panel C. The slope the fitted line is -0.48% correlation component change per year relative to value at age 0. r^2 values (variance accounted for by the linear model) are included in insets in panels C and D for comparison to r^2 values reported in Fig. 8.

Table 4
Significance testing of CDR stage on covariance and correlation components. $\boldsymbol{\Delta\bar{\Psi}}_*$ and $\boldsymbol{\Delta\bar{\psi}}_*$ represent, respectively, covariance and correlation component differences contrasting participant subgroup vs. controls. All comparisons are based on data from which the effects of age and cohort have been removed by regression. The test statistic is the L1-norm of component differences. Within AD cohort differences are relative to controls. Between cohort differences are as labeled. Significance was estimated by comparison of the true test statistic against the distribution of nulls obtained by 100,000-fold permutation resampling. The listed *p*-values are not corrected for multiple comparisons. *p*-values < 0.05 are highlighted.

Within Cohort Contrasts			$\lvert\boldsymbol{\Delta\bar{\Psi}}_*\rvert$ p-value	$\lvert\boldsymbol{\Delta\bar{\psi}}_*\rvert$ p-value
WUSM	LOAD Aβ+	CDR 0	0.734	0.859
cohort		CDR 0.5	0.566	0.236
		CDR 1+	0.00024	$<10^{-10}$
DIAN	Aβ-	CDR 0	0.589	0.971
Mutation+	Aβ+	CDR 0	0.984	0.919
cohort		CDR 0.5	0.383	0.156
		CDR 1+	0.045	$<10^{-5}$
Between Cohort Contrasts			$\lvert\boldsymbol{\Delta\bar{\Psi}}_*\rvert$ p-value	$\lvert\boldsymbol{\Delta\bar{\psi}}_*\rvert$ p-value
WUSM vs. DIAN Aβ+ CDR 0			0.785	0.875
WUSM vs. DIAN Aβ+ CDR 0.5			0.808	0.609
WUSM vs. DIAN Aβ+ CDR 1+			0.707	0.034

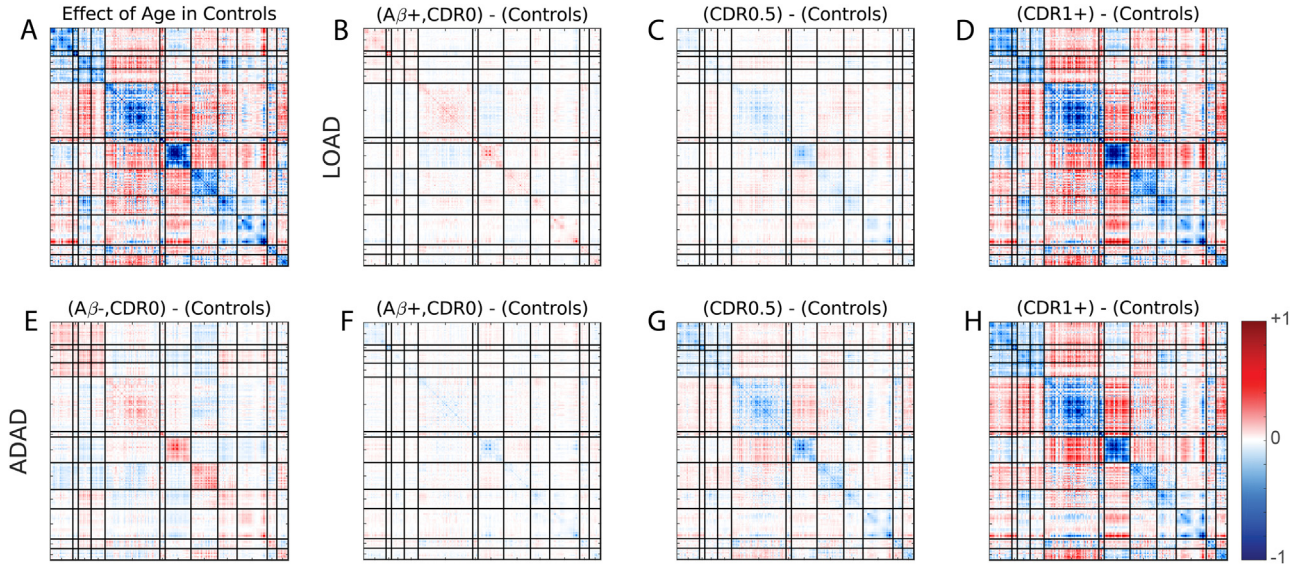

Fig. 6. Covariance FC matrix changes with age, ADAD, and LOAD. In Panel A, the effect of age (Fig. 5A) has been multiplied by 35 years, which is the mean age difference in the DIAN vs. WUSM controls. Panels B-D and F-H show Aβ positive CDR 0, CDR 0.5 and CDR 1+ vs. control, dimensionality reduced, difference matrices in the WUSM and DIAN participants, respectively, evaluated as $\hat{\mathbf{W}}\Delta\bar{\mathbf{\Psi}}_*\hat{\mathbf{W}}^{\mathbf{T}}$. The effects of age and cohort have removed from the AD results. Note consistent "matrix topography" with variable scaling, i.e., absence of CDR-dependent focality evident on inspection. Corresponding undifferenced covariance and correlation matrices are shown in Fig. S4. Matrix block labels are identical to those in Figs. 3 and 4; they are omitted here to optimize use of space.

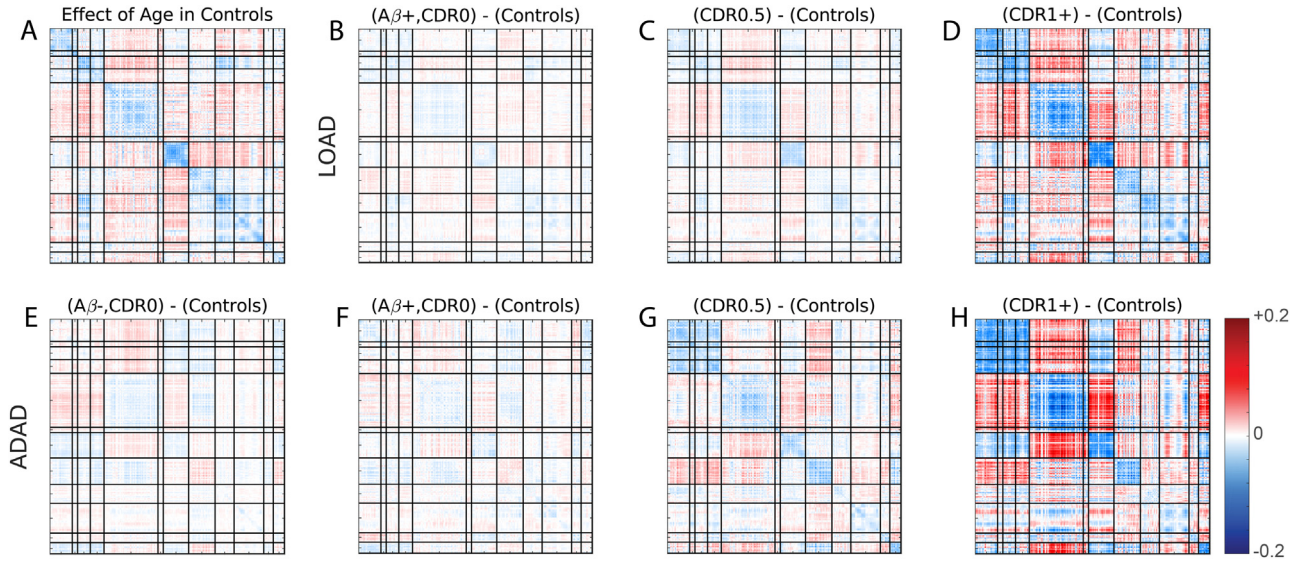

Fig. 7. Correlation FC matrix changes with age, ADAD, and LOAD. This figure is parallel to Fig. 6. The effect of age (Panel A) has been multiplied by 35 years as in Fig. 6. Panels B-D and F-H show Aβ positive CDR 0, CDR 0.5 and CDR 1+ vs. control, dimensionally reduced, difference matrices in the WUSM and DIAN participants, respectively, evaluated as $\hat{\mathbf{w}}\Delta\bar{\boldsymbol{\psi}}_*\hat{\mathbf{w}}^{\mathbf{T}}$. Correlation values have been scaled by $\upsilon_{\mathbf{CONT}} = 2.98$ to facilitate comparison with parallel covariance results shown in Fig. 6. Again, note consistent "matrix topography" with variable scaling. Corresponding undifferenced covariance and correlation matrices are shown in Fig. S5.

Panels D - F show correlation component results. Panel D relates change in component value per year (β_j^{Age}) to baseline component values extrapolated to age 0 (β_j^{Int}) in a manner parallel to panel A. Panels D and E show correlation component differences (CDR 1+ minus control) for LOAD ($\Delta\bar{\Psi}_j$) and ADAD ($\Delta\bar{\psi}_j$) parallel to panels B and C. Correlation components depart from the regression line more than corresponding covariance components. Quantitative measures of departure from the fitted line (squared Pearson correlation) are reported as insets in each panel. These results indicate that correlation FC shows more evidence of focality in AD than does covariance FC. However, plotting ADAD $\Delta\bar{\psi}_j$ vs. LOAD $\Delta\bar{\psi}_j$ (panel F) reveals little evidence of differential ADAD vs. LOAD focality (Pearson correlation = 0.872), as in panel C. However, the difference in slopes of the fitted lines (1.17 vs. 0.75) suggests that, as assessed at CDR 1+, ADAD leads to more pronounced correlation FC differences relative to controls than does LOAD. A direct test of this contrast yielded a formally significant result (Table 4, uncorrected for multiple comparisons).

4. Discussion

4.1. Results overview

We contrasted age, ADAD, and LOAD using dimensionality reduced covariance FC and correlation FC projections onto fixed bases. Comparison of dimensionally reduced covariance vs. correlation FC at the group level revealed that these two measures are, to a good approximation,

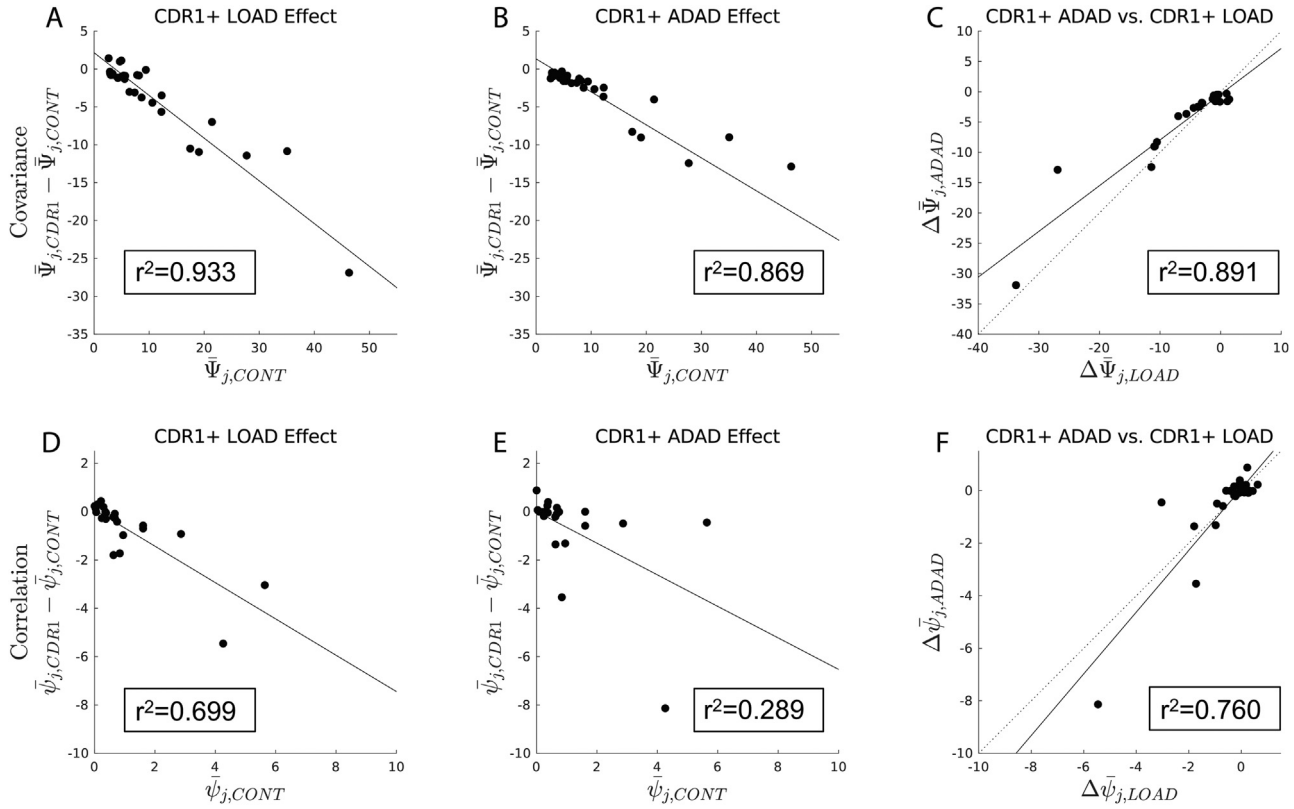

Fig. 8. Change in covariance and correlation component values with LOAD and ADAD at CDR 1+. Each panel includes 30 symbols corresponding to the dimensionality of the fixed bases. Panels A and B show CDR 1+ LOAD and ADAD covariance component differences relative to controls. $\mathbf{\Delta\bar{\Psi}_j}$ is the mean CDR1+ vs. mean control difference in the $\mathbf{j^{th}}$ covariance component. Plotting $\mathbf{\Delta\bar{\Psi}_j}$ vs. $\mathbf{\bar{\Psi}_{j,CONT}}$ visualizes differences relative to controls vs. the control mean, i.e., proportional differences. Insets report r^2 (fraction of variance accounted for by the linear model), i.e., extent to which all components exhibit the same proportional difference at CDR 1+ relative to controls. Non-proportional differences indicate the presence of focality. Panel C plots $\mathbf{\Delta\bar{\Psi}_j}$ for ADAD vs. $\mathbf{\Delta\bar{\Psi}_j}$ for LOAD. The effects of LOAD and ADAD on covariance FC are very strongly correlated (r^2=0.891). The line of identity is dotted. Panels D - F show correlation component results parallel to panels A - C (omitting υ_*). $\mathbf{\Delta\bar{\psi}_j}$ is the mean CDR1+ vs. mean control difference in the $\mathbf{j^{th}}$ correlation component. Deviation from the linear fit in panels D and E is evident, most markedly in the strongest two correlation components. Thus, focality in the effects of AD on functional connectivity is more evident in correlation FC as opposed to covariance FC. Panel F is exactly parallel to panel C. The strong Pearson correlation (r^2=0.760) suggests approximately comparable effects of LOAD and ADAD on correlation FC.

related by a scalar proportionality factor, in controls as well as AD-affected participants. Three principal results emerged: (1) Healthy aging leads to global loss of rs-fMRI covariance with little or no evidence that specific RSNs are particularly affected. Hence, conventional correlation FC is comparatively unaffected by healthy aging, as previously reported (Brier et al., 2014). (2) In contrast, both LOAD and ADAD lead to marked changes in both correlation and covariance FC, but only at CDR 1+. The global covariance:correlation ratio (υ) systematically declines in association with clinical progression. (3) 3-way ANOVA of covariance FC ($\Delta\bar{\Psi}_*$), parametric in CDR stage returned no statistically significant difference between ADAD and LOAD (Table S2). This result supports a schema in which ADAD is regarded as a model of LOAD (Bateman et al., 2011). However, systematic evaluation of the global covariance:correlation proportionality ratio (υ_*) suggests that loss of BOLD signal amplitude is accelerated in ADAD relative to LOAD (Tables 3 and 4).

4.2. Methodology

Computing both covariance and correlation FC confers enhanced interpretability of resting state fMRI studies (Cole et al., 2016; Duff et al., 2018). This principle has been applied mostly in studies contrasting task or arousal states within individuals, e.g., (Bijsterbosch et al. 2017, Duff et al. 2018). We have recently applied parallel covariance + correlation analysis to a longitudinal study of the effects of mindfulness training and exercise in older individuals (Snyder et al., 2022). Here, we apply this methodology to a cross-sectional study.

Our approach to covariance analysis assumes a common structure across individuals (Varoquaux et al., 2010), which corresponds to the "average" model in the classification scheme of Madsen et al. (2017). Thus, the methodology *per se* is not novel. However, It is noteworthy that group-averaged covariance and correlation matrices exhibit similar structure (Figs. 4; S4; S5), a result that has been obtained before (Cole et al., 2016). It is this similarity that enables defining the global covariance:correlation proportionality scalar (υ). In should be noted that covariance FC theoretically is sensitive to individual variability in the anatomical distribution of functional systems in a manner that correlation FC is not. Potential mechanisms include anatomical variability (despite non-linear atlas registration), individual differences in the representation of function in relation to gyral anatomy (Gordon et al., 2017) and variation in neurovascular coupling (Hillman 2014). Appendix C models this effect as inter-individual differences in "ROI-level gain variability". Numerical simulations over a range additive noise levels empirically show that such differences average out at the group level (Fig. S6).

The present work applies well-established linear algebraic tools (dimensionality reduction and projection) to FC analysis. The principal advantage of analyzing group differences in terms of components is dimensionality reduction, hence, preservation of statistical power in data-driven analyses. Fig. 2 shows that a 30-component basis provides a nearly complete representation rs-fMRI covariance at the level of functional systems. Projection of FC onto a space of relatively low dimension should be distinguished from dimensionality-preserving approaches to

FC analysis that require regularization of matrix inversion (Brier et al., 2015; Rahim et al., 2017). Figs. 2 and 3 suggest that 30 components are sufficient to capture the principal features of resting state fMRI covariance matrices, i.e., hierarchical structure of limited dimensionality (Cordes and Nandy 2006; Laumann et al., 2017; Gotts et al., 2020). The projection strategy reduces the computational complexity of cross-group comparisons (Figs. 5–8) and enables use of straightforward regression techniques to separate the effects of age vs. pathology while controlling for technical differences between participant cohorts (e.g., scanners and sequences). While the analysis algebra (principal component analysis and linear regression) is not novel, parallel covariance/correlation analysis facilitates new inferences concerning aging vs. AD.

4.3. Covariance and correlation FC functional connectivity in healthy aging

Perhaps the most striking present finding is the uniformity, i.e., non-focality, of the age effect across covariance components (Fig. 5C). Across all components, change per year relative to value extrapolated to age 0 (B_j^{Age}/B_j^{Int}) is remarkably constant across components. The fitted line indicates ~1.69% loss per year relative to starting value, estimated on basis of data in participants over the age range contributing to the model (Fig. S3). We recently reported similarly broad, age-related reductions in BOLD fMRI signal variability in the cognitively intact subset of the LOAD cohort (Millar et al., 2020). The present analysis differs in that we include the control component of the DIAN cohort as well and, crucially, exclude from the aging analysis participants with imaging evidence of pre-clinical AD (Brier et al., 2014). Age-related loss of BOLD signal covariance is consistent with previous findings reported as multifocal changes in the temporal standard deviation of fMRI data (SD_{BOLD}) (Garrett et al., 2010; Grady and Garrett 2014; Vieira et al., 2020; Hrybouski et al., 2021). Fig. 5C suggests that this phenomenon is anatomically global as opposed to multifocal.

Theoretically, if all covariance components proportionally attenuate with age, there should be no effect of age on correlation FC, as discussed in Appendix B. Fig. 5 shows that there is an effect of age on correlation FC but it is quantitatively minor in comparison to the effect of moderately advanced AD (see Section 4.4). This result essentially confirms our prior finding that correlation FC is minimally affected by age in older individuals without imaging evidence of preclinical AD (Brier et al., 2014). Modest focality in age-related change in correlation components may be present in the control participants (Fig. 5D). Screening for preclinical AD on the basis of Aβ and tau does not exclude other predisposing factors, e.g., family history of AD (Wang et al., 2012). Thus, it is possible that low doses of pathology with effects similar to Aβ/tau or any age-associated condition, e.g., vascular disease, also affected the control participants. Viewed from this perspective, the results shown Fig. 5D are consistent with prior reports of age-related changes in correlation FC in cognitively normal older adults, none of which included any screening to exclude sub-clinical AD (Andrews-Hanna et al., 2007; Dennis and Thompson 2014; Sala-Llonch et al., 2015).

Several potential mechanisms may account for age-related loss of spontaneous BOLD signal fluctuation amplitude. In principle, age-related atrophy could be a contributing factor. However, cross-sectional anatomical studies of healthy young vs. older adults report that cortical thickness changes by only ~0.1–0.2% per year over the lifespan (Salat et al., 2004; Bakkour et al., 2013). This small figure does not account for age-related loss of BOLD signal fluctuations even if the present finding of signal power loss is expressed in terms of amplitude (divide 1.69% by 2). Whole brain atrophy has been estimated as 0.5% volume loss per year between ages 59 and 85 (Resnick et al., 2003). This figure comes closer to accounting for loss of intrinsic BOLD signal fluctuations but raises the question of whether age-associated white matter atrophy and cerebrovascular disease play a role. Indeed, it has been reported that white matter disease degrades FC within specific RSNs (Teipel et al., 2010; Fjell et al., 2017). It appears likely that age-related changes in metabolic and molecular processes are related to loss of BOLD signal fluctuations (Bishop et al., 2010; Peng et al., 2014). Whole brain glucose utilization is about ~20% lower in cognitively intact older adults (age ~75 years) as compared to young adults (age ~25 years) (Goyal et al., 2017).

4.4. Covariance and correlation functional connectivity in LOAD and ADAD

In contrast to healthy aging, AD (both variants) leads to markedly altered correlation FC (Figs. 6–8). We find no statistically reliable FC abnormalities at CDR stage < 1 (Ibrahim et al., 2021). This result supports the growing consensus that, unlike Aβ/tau PET and structural imaging (Gordon et al., 2019), conventional correlation analysis of resting state fMRI is unlikely to provide an early biomarker of AD. This perspective is implicit in a recent authoritative review of the topic (Hampel et al., 2021). On the other hand, the close temporal association of FC abnormalities with clinical dementia implies that resting state BOLD fMRI is useful in assessing the functional status of the brain, albeit with limited etiologic specificity: AD is only one of any number of diverse entities that impair cognition in association with FC abnormalities (Zhang et al., 2021). Apart from altered FC, rs-fMRI features that distinguish CDR 1+ participants from controls include a lower value of the global covariance:correlation proportionality scalar (υ; Table 3) and departures from proportional correlation FC component changes relative to controls ($\Delta\bar{\psi}$; Fig. 8D,E). A low value of υ with maintained $\langle\hat{C}\rangle_k$:$\langle\hat{r}\rangle_k$correlation (η; Table 3) implies loss of BOLD signal fluctuation amplitude in excess of degraded RSN structure. This finding is consistent with prior reports of reduced ALFF in AD (Yang et al., 2018; Zeng et al., 2019). BOLD signal fluctuation amplitude, cerebral blood flow, and glucose metabolism all are closely linked in healthy brains (Wang et al., 2021) as well as in brains affected by AD (Marchitelli et al., 2018). Thus, loss of BOLD signal fluctuation amplitude is an expected correlate of reduced metabolism in AD. Pathology and atrophy are quantitatively greater and spatially more extensive in ADAD in comparison to LOAD (Cairns et al., 2015; Ringman et al., 2016; Dincer et al., 2020). This difference may underlie the ADAD vs. LOAD $|\Delta\bar{\psi}_*|$ finding (Table 4) and possibly the accelerated change in υ_* (Table 3). The results reported in Table 3 reinforce the recent observation that loss of ALFF is correlated with Aβ burden (Scheel et al., 2022).

Fig. 8 suggests that there exists a dissociation between correlation vs. covariance FC in the degree of non-uniformity over components (i.e., departure from linear fit; panels D,E vs. A,B). This finding implies that RSN-specific abnormalities are more prominent in conventional correlation FC as opposed to covariance FC. This inference is consistent with the existence of multiple prior papers describing focal or RSN-specific FC abnormalities in AD, e.g., (Buckner et al. 2005, Brier et al. 2012, Toepper 2017, Chhatwal et al. 2018, Lin et al. 2018). A parsimonious account of differential correlation vs. covariance focality can be formulated by invoking a distinction between widely shared vs. locally restricted signals (Cole et al., 2016)(Appendix B). This approach to disambiguating FC has been alternatively articulated in terms of Additive Signal Change theory (Duff et al., 2018). Thus, because locally restricted signals (in the nomenclature of Appendix B) do not contribute to covariance but do depress Pearson correlation, differential correlation vs. covariance FC focality can arise from an uneven distribution of locally restricted signals over the brain. The results shown in Fig. 8 suggest that this may occur in moderately advanced AD. We do not attempt here to detail which RSNs or brain regions are particularly susceptible to developing locally restricted signals as that analysis, as well as detailing local deviations from scalar covariance:correlation proportionality (Fig. 4C), falls outside the scope of the present work.

4.5. rs-fMRI functional connectivity as a means of localizing pathology

The notion that there exists an topographic correspondence between AD histopathology and FC changes arguably dates back to 2004, when

Greicius and colleagues reported that AD patients could be separated from non-demented controls on the basis of DMN functional connectivity (Greicius et al., 2004). The inference was compelling as impaired memory is the hallmark of AD while the DMN is the RSN most associated with memory (Buckner and DiNicola 2019). The link was subsequently reinforced by several papers highlighting the spatial overlap between the DMN and Aβ accumulation as imaged by PiB-PET (Buckner et al., 2005). Importantly, Greicius and colleagues did not claim that AD affects only the DMN. It has since become clear that multiple RSNs are affected (Sheline et al., 2010; Brier et al., 2012; Fjell et al., 2015; Franzmeier et al., 2020; Ripp et al., 2020).

Nevertheless, the topographic correspondence between histopathology and FC abnormalities in AD is not as straightforward as once seemed. The staging of neuropathology in AD is well documented (Braak et al., 2011). Crucially, primary sensory cortices are spared until later stages of the disease. The distribution of pathology in both LOAD and ADAD (Aβ/tau deposition, lower flouro-deoxyglucose uptake, atrophy) similarly spares primary sensorimotor areas (Brier et al., 2016; Hansson and Gouras 2016; Gordon et al., 2019). This does not match rs-fMRI findings (Figs. 6 and 7, panels D and H). Although the DMN is affected at CDR 1+ in both LOAD and ADAD, somatomotor, cingulo-opercular and auditory cortices are comparably affected and the greatest loss of covariance FC occurs in visual areas. Thus, there exists a substantial discrepancy between the distribution of histopathology vs. the distribution of FC changes. A similar discrepancy exists in Parkinson disease (Gratton et al., 2019). The physiological significance of this discrepancy remains to be determined but the available evidence excludes a straightforward relationship between FC changes and the anatomical distribution of histopathology.

4.6. Caveats and limitations

Projection of rs-fMRI data onto a fixed space of reduced dimensionality constitutes a key feature of the present analysis. This approach implicitly ignores features of rs-fMRI correlation structure outside the fixed projection (formally, the column space of $\hat{W}$ and $\hat{w}$). However, as shown in Fig. S5, the fixed bases reasonably well represent the covariance and correlation structures of participant subgroups. Hypothetically, the present approach to dimensionality reduction could miss meaningful group differences outside the projection. However, Fig. 2 shows that the hierarchical structure of group-level RSNs is almost completely captured by 30 components representing 222 ROIs. Thus, if the present analysis has missed important FC features, they would have to exist at a granularity finer than the block structure illustrated in Fig. 2. Additionally, we note that the effects of aging in healthy individuals as well as CDR stage have been inferred on the basis of exclusively cross-sectional data. Finally, the sensitivity of certain group comparisons is limited by the sample size of CDR 1+ participants (Table 1). We plan to update the analyses as larger samples become available.

Code and data availability statement

The primary data analyzed in this study were obtained by the Washington University Alzheimer Disease Research Center (ADRC; PI: John C. Morris) and the Dominantly Inherited Alzheimer Network (DIAN: PI: Randall J. Bateman). These data may be made available to qualified investigators by request to the ADRC and DIAN PIs. Image processing used the 4dfp suite of analysis tools; 4dfp code is available upon reasonable request to the corresponding author. Matlab code used for algebraic and statistical analyses may be available upon request to Matthew R. Brier.

Declaration of Competing Interest

Randall J. Bateman

Randall Bateman (RJB), Professor of Neurology at Washington University's School of Medicine (WUSM) receives lab research funding from the National Institutes of Health, Alzheimer's Association, BrightFocus Foundation, Rainwater Foundation Tau Consortium, Association for Frontotemporal Degeneration, the Cure Alzheimer's Fund, Centene Corporation, Tau SILK Consortium (AbbVie, Biogen, and Eli Lilly and Company), and an anonymous organization. RJB has received honoraria as a speaker/consultant/advisory board member from Amgen, AC Immune, Eisai, F. Hoffman-LaRoche, and Janssen; and reimbursement of travel expenses from AC Immune, F. Hoffman-La Roche and Janssen.

Unrelated to this article, RJB serves as principal investigator of the DIAN-TU, which is supported by the Alzheimer's Association, GHR Foundation, an anonymous organization and the DIAN-TU Pharma Consortium (Active: Eli Lilly and Company/Avid Radiopharmaceuticals, F. Hoffman-La Roche/Genentech, Biogen, Eisai, Janssen, and United Neuroscience. Previous: Abbvie, Amgen, AstraZeneca, Forum, Mithridion, Novartis, Pfizer, Sanofi). The DIAN-TU-001 Clinical Trial is supported by Pharmaceutical Partners Eli Lilly and Company, F. Hoffman-La Roche and Janssen, the Alzheimer's Association, NIH U01AG042791, NIH U01AG42791-S1 (FNIH and Accelerating Medicines Partnership), NIH R01AG046179, NIH R56AG053267, NIH R01AG053267, NIH U01AG059798, NIH R01AG068319, Avid Radiopharmaceuticals, GHR Foundation, and an anonymous organization. In-kind support has been received from CogState and Bracket.

Washington University, Randall Bateman, and David Holtzman have equity ownership interest in C2N Diagnostics and receive royalty income based on technology (stable isotope labeling kinetics and blood plasma assay) licensed by Washington University to C2N Diagnostics. RJB receives income from C2N Diagnostics for serving on the scientific advisory board. Washington University, with RJB as co-inventor, has submitted the US nonprovisional patent application "Methods for Measuring the Metabolism of CNS Derived Biomolecules *In Vivo*" and provisional patent application "Plasma Based Methods for Detecting CNS Amyloid Deposition".

Tammie L.S. Benzinger

Dr. Benzinger reports grants and non-financial support from Avid Radiopharmaceuticals/ Eli Lilly, during the conduct of the study; grants and non-financial support from Avid Radiopharmaceuticals/ Eli Lilly, other from Eli Lilly, Biogen, Eisai, Jaansen, personal fees from Biogen, non-financial support from Eisai, non-financial support from Siemens, outside the submitted work.

Matthew R. Brier

Dr. Brier reports grants from NIH, during the conduct of the study.

Gregory S. Day

Dr. Day reports grants from NIH, during the conduct of the study; personal fees from Parabon Nanolabs, Inc, personal fees from DynaMed (EBSCO Health), outside the submitted work.

Brian A. Gordon

Dr. Gordon reports participation in clinical trials of therapies to alter the course of Alzheimer Disease.

Neill Graff-Radford

Dr. Graff-Radford reports grants from NIH, during the conduct of the study; grants from Biogen, grants from AbbVie, grants from Lilly, outside the submitted work.

Taleshi Ikeuchi

Dr. Ikeuchi reports grants from AMED (Japan Agency for Medical Research and Development), during the conduct of the study.

Daniel S. Marcus

Dr. Marcus reports other from Radiologics, Inc, outside the submitted work.

John C. Morris

Dr. Morris reports grants from NIH grant P30 AG066444, grants from NIH grant P01AG003991, grants from NIH grant P01AG026276, grants from NIH grant UF1AG032438, during the conduct of the study.

Richard J. Perrin Dr. Perrin reports grants from NIH during the conduct of the study.

Stephen Salloway

Dr. Salloway reports grants and personal fees from Biogen, grants and personal fees from Eisai, grants and personal fees from Avid, grants and personal fees from Lilly, personal fees from Genentech, personal fees from Novartis, grants and personal fees from Roche, outside the submitted work.

Peter Schofield

Dr. Schofield reports grants from NIH, grants from Anonymous Foundation, grants from Roth Charitable Foundation, during the conduct of the study.

Abraham Z. Snyder

Dr. Snyder is a consultant for Sora Neuroimaging, LLC.

Credit authorship contribution statement

Jeremy F. Strain: Formal analysis, Writing – original draft, Writing – review & editing. **Matthew R. Brier:** Formal analysis, Writing – original draft, Writing – review & editing. **Aaron Tanenbaum:** Formal analysis, Writing – review & editing. **Brian A. Gordon:** Writing – original draft, Writing – review & editing. **John E. McCarthy:** Writing – original draft, Writing – review & editing. **Aylin Dincer:** Formal analysis, Writing – review & editing. **Daniel S. Marcus:** Funding acquisition, Data curation, Writing – review & editing. **Jasmeer P. Chhatwal:** Funding acquisition, Data curation, Writing – review & editing. **Neill R. Graff-Radford:** Visualization, Funding acquisition, Data curation, Writing – review & editing. **Gregory S. Day:** Visualization, Writing – original draft, Writing – review & editing. **Christian la Fougère:** Visualization, Writing – original draft, Writing – review & editing. **Richard J. Perrin:** Visualization, Writing – original draft, Writing – review & editing. **Stephen Salloway:** Visualization, Writing – review & editing. **Peter R. Schofield:** Visualization, Writing – original draft, Writing – review & editing. **Igor Yakushev:** Funding acquisition, Data curation, Writing – review & editing. **Takeshi Ikeuchi:** Visualization, Writing – original draft, Writing – review & editing. **Jonathan Vöglein:** Visualization, Writing – review & editing. **John C. Morris:** Visualization, Writing – original draft, Writing – review & editing. **Tammie L.S. Benzinger:** Visualization, Funding acquisition, Data curation, Writing – review & editing. **Randall J. Bateman:** Visualization, Writing – review & editing. **Beau M. Ances:** Visualization, Writing – original draft, Writing – review & editing. **Abraham Z. Snyder:** Formal analysis, Writing – original draft, Writing – review & editing.

Acknowledgments

This work would not have been possible without the dedication and contribution from our participants. We thank all affiliated partners that comprise the Dominantly Inherited Alzheimer Network. Ben Seitzman prepared Fig. 1. This research was funded by the National Institutes of Health (NIH: K01AG053474, UFAG032438, UL1TR000448, P30NS098577, R01EB009352, R01NR012907, R01NR012657, R01NR014449, P50AG05681, P01AG003991, P30AG066444, P01AG03991, P01AG026276, P30NS048056, R01AG04343404, R01AG062667, R01AG052550, P01AG036694, 2R25NS090978-06, R01AG05255001A1, R25NS090978-06), NSF DMS grant 2054199, the German Center for Neurodegenerative Diseases (DZND), the National institute for Health Research (NIHR) Queen Square Dementia Biomedical Research Centre, and the Medical Research Council Dementias Platform UK (MR/L023784/1 and MR/009076/1), AMED JP21dk0207049. Data collection and sharing for this project was supported by The Dominantly Inherited Alzheimer Network (DIAN, UF1AG032438) funded by the National Institute on Aging (NIA), the German Center for Neurodegenerative Diseases (DZNE). We acknowledge the altruism of the participants and their families and contributions of the DIAN research and support staff at each of the participating sites for their contributions to this study. We acknowledge the financial support of Fred Simmons and Olga Mohan, the Barnes-Jewish Hospital Foundation, the Charles F. and Joanne Knight Alzheimer research Initiative, the Hope Center for Neurological Disorders, the Mallinckrodt Institute of Radiology, the Daniel Brennan MD Fund, the Roth Charitable Foundation, the Doris Duke Charitable Foundation, and the Paula and Rodger O. Riney Fund.

Supplementary materials

Supplementary material associated with this article can be found, in the online version, at doi:10.1016/j.neuroimage.2022.119511.

References

Almkvist, O., Rodriguez-Vieitez, E., Thordardottir, S., Amberla, K., Axelman, K., Basun, H., Kinhult-Stahlbom, A., Lilius, L., Remes, A., Wahlund, L.O., Viitanen, M., Lannfelt, L., Graff, C., 2017. Predicting cognitive decline across four decades in mutation carriers and non-carriers in autosomal-dominant Alzheimer's disease. J. Int. Neuropsychol. Soc. 23 (3), 195–203.

Andersson, J.L.R., Jenkinson M. and Smith S. (2010). FMRIB Technical report TR07JA2.

Andrews-Hanna, J.R., Snyder, A.Z., Vincent, J.L., Lustig, C., Head, D., Raichle, M.E., Buckner, R.L., 2007. Disruption of large-scale brain systems in advanced aging. Neuron 56 (5), 924–935.

Bakkour, A., Morris, J.C., Wolk, D.A., Dickerson, B.C., 2013. The effects of aging and Alzheimer's disease on cerebral cortical anatomy: specificity and differential relationships with cognition. Neuroimage 76, 332–344.

Bateman, R.J., Aisen, P.S., De Strooper, B., Fox, N.C., Lemere, C.A., Ringman, J.M., Salloway, S., Sperling, R.A., Windisch, M., Xiong, C., 2011. Autosomal-dominant Alzheimer's disease: a review and proposal for the prevention of Alzheimer's disease. Alzheimers Res. Ther. 3 (1), 1.

Bateman, R.J., Xiong, C., Benzinger, T.L., Fagan, A.M., Goate, A., Fox, N.C., Marcus, D.S., Cairns, N.J., Xie, X., Blazey, T.M., Holtzman, D.M., Santacruz, A., Buckles, V., Oliver, A., Moulder, K., Aisen, P.S., Ghetti, B., Klunk, W.E., McDade, E., Martins, R.N., Masters, C.L., Mayeux, R., Ringman, J.M., Rossor, M.N., Schofield, P.R., Sperling, R.A., Salloway, S., Morris, J.C., Dominantly Inherited Alzheimer, N., 2012. Clinical and biomarker changes in dominantly inherited Alzheimer's disease. N. Engl. J. Med. 367 (9), 795–804.

Behzadi, Y., Restom, K., Liau, J., Liu, T.T., 2007. A component based noise correction method (CompCor) for BOLD and perfusion based fMRI. Neuroimage 37 (1), 90–101.

Bijsterbosch, J., Harrison, S., Duff, E., Alfaro-Almagro, F., Woolrich, M., Smith, S., 2017. Investigations into within- and between-subject resting-state amplitude variations. Neuroimage 159, 57–69.

Bishop, N.A., Lu, T., Yankner, B.A., 2010. Neural mechanisms of ageing and cognitive decline. Nature 464 (7288), 529–535.

Braak, H., Thal, D.R., Ghebremedhin, E., Del Tredici, K., 2011. Stages of the pathologic process in Alzheimer disease: age categories from 1 to 100 years. J. Neuropathol. Exp. Neurol. 70 (11), 960–969.

Brier, M.R., Gordon, B., Friedrichsen, K., McCarthy, J., Stern, A., Christensen, J., Owen, C., Aldea, P., Su, Y., Hassenstab, J., Cairns, N.J., Holtzman, D.M., Fagan, A.M., Morris, J.C., Benzinger, T.L., Ances, B.M., 2016. Tau and Abeta imaging, CSF measures, and cognition in Alzheimer's disease. Sci. Transl. Med. 8 (338), 338–366.

Brier, M.R., Mitra, A., McCarthy, J.E., Ances, B.M., Snyder, A.Z., 2015. Partial covariance based functional connectivity computation using Ledoit-Wolf covariance regularization. Neuroimage 121, 29–38.

Brier, M.R., Thomas, J.B., Snyder, A.Z., Benzinger, T.L., Zhang, D., Raichle, M.E., Holtzman, D.M., Morris, J.C., Ances, B.M., 2012. Loss of intranetwork and internetwork resting state functional connections with Alzheimer's disease progression. J. Neurosci. 32 (26), 8890–8899.

Brier, M.R., Thomas, J.B., Snyder, A.Z., Wang, L., Fagan, A.M., Benzinger, T., Morris, J.C., Ances, B.M., 2014. Unrecognized preclinical Alzheimer disease confounds rs-fcMRI studies of normal aging. Neurology 83 (18), 1613–1619.

Buckner, R.L., DiNicola, L.M., 2019. The brain's default network: updated anatomy, physiology and evolving insights. Nat. Rev. Neurosci. 20 (10), 593–608.

Buckner, R.L., Snyder, A.Z., Shannon, B.J., LaRossa, G., Sachs, R., Fotenos, A.F., Sheline, Y.I., Klunk, W.E., Mathis, C.A., Morris, J.C., Mintun, M.A., 2005. Molecular, structural, and functional characterization of Alzheimer's disease: evidence for a relationship between default activity, amyloid, and memory. J. Neurosci. 25 (34), 7709–7717.

Cairns, N.J., Perrin, R.J., Franklin, E.E., Carter, D., Vincent, B., Xie, M., Bateman, R.J., Benzinger, T., Friedrichsen, K., Brooks, W.S., Halliday, G.M., McLean, C., Ghetti, B., Morris, J.C., 2015. Neuropathologic assessment of participants in two multi-center longitudinal observational studies: the Alzheimer disease neuroimaging initiative (ADNI) and the dominantly inherited Alzheimer network (DIAN). Neuropathology 35 (4), 390–400.

Chhatwal, J.P., Schultz, A.P., Johnson, K.A., Hedden, T., Jaimes, S., Benzinger, T.L.S., Jack, C., Ances, B.M., Ringman, J.M., Marcus, D.S., Ghetti, B., Farlow, M.R., Danek, A., Levin, J., Yakushev, I., Laske, C., Koeppe, R.A., Galasko, D.R., Xiong, C., Masters, C.L., Schofield, P.R., Kinnunen, K.M., Salloway, S., Martins, R.N., McDade, E., Cairns, N.J., Buckles, V.D., Morris, J.C., Bateman, R., Sperling, R.A., 2018. Preferential degradation of cognitive networks differentiates Alzheimer's disease from ageing. Brain 141 (5), 1486–1500.

Cole, M.W., Yang, G.J., Murray, J.D., Repovs, G., Anticevic, A., 2016. Functional connectivity change as shared signal dynamics. J. Neurosci. Methods 259, 22–39.

Cordes, D., Nandy, R.R., 2006. Estimation of the intrinsic dimensionality of fMRI data. Neuroimage 29 (1), 145–154.

Damoiseaux, J.S., 2017. Effects of aging on functional and structural brain connectivity. Neuroimage 160, 32–40.
Dennis, E.L., Thompson, P.M., 2014. Functional brain connectivity using fMRI in aging and Alzheimer's disease. Neuropsychol. Rev. 24 (1), 49–62.
Dincer, A., Gordon, B.A., Hari-Raj, A., Keefe, S.J., Flores, S., McKay, N.S., Paulick, A.M., Shady Lewis, K.E., Feldman, R.L., Hornbeck, R.C., Allegri, R., Ances, B.M., Berman, S.B., Brickman, A.M., Brooks, W.S., Cash, D.M., Chhatwal, J.P., Farlow, M.R., la Fougere, C., Fox, N.C., Fulham, M.J., Jack, C.R., Joseph-Mathurin, N., Karch, C.M., Lee, A., Levin, J., Masters, C.L., McDade, E.M., Oh, H., Perrin, R.J., Raji, C., Salloway, S.P., Schofield, P.R., Su, Y., Villemagne, V.L., Wang, Q., Weiner, M.W., Xiong, C., Yakushev, I., Morris, J.C., Bateman, R.J., 2020. Comparing cortical signatures of atrophy between late-onset and autosomal dominant Alzheimer disease. Neuroimage . 28, 102491.
Duff, E.P., Makin, T., Cottaar, M., Smith, S.M., Woolrich, M.W., 2018. Disambiguating brain functional connectivity. Neuroimage 173, 540–550.
Ferreira, L.K., Busatto, G.F., 2013. Resting-state functional connectivity in normal brain aging. Neurosci. Biobehav. Rev. 37 (3), 384–400.
Fischl, B., 2012. FreeSurfer. Neuroimage 62 (2), 774–781.
Fjell, A.M., Sneve, M.H., Grydeland, H., Storsve, A.B., Amlien, I.K., Yendiki, A., Walhovd, K.B., 2017. Relationship between structural and functional connectivity change across the adult lifespan: a longitudinal investigation. Hum. Brain Mapp. 38 (1), 561–573.
Fjell, A.M., Sneve, M.H., Grydeland, H., Storsve, A.B., de Lange, A.G., Amlien, I.K., Rogeberg, O.J., Walhovd, K.B., 2015. Functional connectivity change across multiple cortical networks relates to episodic memory changes in aging. Neurobiol. Aging 36 (12), 3255–3268.
Forouzannezhad, P., Abbaspour, A., Fang, C., Cabrerizo, M., Loewenstein, D., Duara, R., Adjouadi, M., 2019. A survey on applications and analysis methods of functional magnetic resonance imaging for Alzheimer's disease. J. Neurosci. Methods 317, 121–140.
Franzmeier, N., Neitzel, J., Rubinski, A., Smith, R., Strandberg, O., Ossenkoppele, R., Hansson, O., 2020. Functional brain architecture is associated with the rate of tau accumulation in Alzheimer's disease. Nat. Commun. 11 (1), 347.
Garrett, D.D., Kovacevic, N., McIntosh, A.R., Grady, C.L., 2010. Blood oxygen level-dependent signal variability is more than just noise. J. Neurosci. 30 (14), 4914–4921.
Gholipour, A., Kehtarnavaz, N., Gopinath, K., Briggs, R., Panahi, I., 2008. Average field map image template for Echo-planar image analysis. In: Proceedings of the Conference IEEE Engineering in Medicine and Biology Society, pp. 94–97.
Gordon, B.A., Blazey, T.M., Christensen, J., Dincer, A., Flores, S., Keefe, S., Chen, C., Su, Y., McDade, E.M., Wang, G., Li, Y., Hassenstab, J., Aschenbrenner, A., Hornbeck, R., Jack, C.R., Ances, B.M., Berman, S.B., Brosch, J.R., Galasko, D., Gauthier, S., Lah, J.J., Masellis, M., van Dyck, C.H., Mintun, M.A., Klein, G., Ristic, S., Cairns, N.J., Marcus, D.S., Xiong, C., Holtzman, D.M., Raichle, M.E., Morris, J.C., Bateman, R.J., Benzinger, T.L.S., 2019. Tau PET in autosomal dominant Alzheimer's disease: relationship with cognition, dementia and other biomarkers. Brain 142 (4), 1063–1076.
Gordon, B.A., Blazey, T.M., Su, Y., Hari-Raj, A., Dincer, A., Flores, S., Christensen, J., McDade, E., Wang, G., Xiong, C., Cairns, N.J., Hassenstab, J., Marcus, D.S., Fagan, A.M., Jack, C.R., Hornbeck, R.C., Paumier, K.L., Ances, B.M., Berman, S.B., Brickman, A.M., Cash, D.M., Chhatwal, J.P., Correia, S., Forster, S., Fox, N.C., Graff-Radford, N.R., la Fougere, C., Levin, J., Masters, C.L., Rossor, M.N., Salloway, S., Saykin, A.J., Schofield, P.R., Thompson, P.M., Weiner, M.M., Holtzman, D.M., Raichle, M.E., Morris, J.C., Bateman, R.J., Benzinger, T.L.S., 2018. Spatial patterns of neuroimaging biomarker change in individuals from families with autosomal dominant Alzheimer's disease: a longitudinal study. Lancet Neurol. 17 (3), 241–250.
Gordon, E.M., Laumann, T.O., Gilmore, A.W., Newbold, D.J., Greene, D.J., Berg, J.J., Ortega, M., Hoyt-Drazen, C., Gratton, C., Sun, H., Hampton, J.M., Coalson, R.S., Nguyen, A.L., McDermott, K.B., Shimony, J.S., Snyder, A.Z., Schlaggar, B.L., Petersen, S.E., Nelson, S.M., Dosenbach, N.U.F., 2017. Precision functional mapping of individual human brains. Neuron 95 (4), 791–807 e797.
Gotts, S.J., Gilmore, A.W., Martin, A., 2020. Brain networks, dimensionality, and global signal averaging in resting-state fMRI: Hierarchical network structure results in low-dimensional spatiotemporal dynamics. Neuroimage 205, 116289.
Goyal, M.S., Vlassenko, A.G., Blazey, T.M., Su, Y., Couture, L.E., Durbin, T.J., Bateman, R.J., Benzinger, T.L., Morris, J.C., Raichle, M.E., 2017. Loss of brain aerobic glycolysis in normal human aging. Cell Metab. 26 (2), 353–360 e353.
Grady, C.L., Garrett, D.D., 2014. Understanding variability in the BOLD signal and why it matters for aging. Brain Imaging Behav. 8 (2), 274–283.
Gratton, C., Koller, J.M., Shannon, W., Greene, D.J., Maiti, B., Snyder, A.Z., Petersen, S.E., Perlmutter, J.S., Campbell, M.C., 2019. Emergent functional network effects in parkinson disease. Cereb. Cortex 29 (6), 2509–2523.
Greicius, M.D., Srivastava, G., Reiss, A.L., Menon, V., 2004. Default-mode network activity distinguishes Alzheimer's disease from healthy aging: evidence from functional MRI, 101, pp. 4637–4642.
Hacker, C.D., Laumann, T.O., Szrama, N.P., Baldassarre, A., Snyder, A.Z., Leuthardt, E.C., Corbetta, M., 2013. Resting state network estimation in individual subjects. Neuroimage 82, 616–633.
Hampel, H., Cummings, J., Blennow, K., Gao, P., Jack, C.R., Vergallo, A., 2021. Developing the ATX(N) classification for use across the Alzheimer disease continuum. Nat. Rev. Neurol. 17 (9), 580–589.
Hansson, O., Gouras, G., 2016. Brain activity and Alzheimer's disease: a complex relationship. Brain 139 (Pt 8), 2109–2110.
Hillman, E.M., 2014. Coupling mechanism and significance of the BOLD signal: a status report. Annu. Rev. Neurosci. 37, 161–181.
Hrybouski, S., Cribben, I., McGonigle, J., Olsen, F., Carter, R., Seres, P., Madan, C.R., Malykhin, N.V., 2021. Investigating the effects of healthy cognitive aging on brain functional connectivity using 4.7 T resting-state functional magnetic resonance imaging. Brain Struct. Funct. 226 (4), 1067–1098.
Ibrahim, B., Suppiah, S., Ibrahim, N., Mohamad, M., Hassan, H.A., Nasser, N.S., Saripan, M.I., 2021. Diagnostic power of resting-state fMRI for detection of network connectivity in Alzheimer's disease and mild cognitive impairment: a systematic review. Hum. Brain Mapp. 42 (9), 2941–2968.
Jalilianhasanpour, R., Beheshtian, E., Sherbaf, G., Sahraian, S., Sair, H.I., 2019. Functional connectivity in neurodegenerative disorders: Alzheimer's disease and frontotemporal dementia. Top. Magn. Reson. Imaging 28 (6), 317–324.
Jenkinson, M., Beckmann, C.F., Behrens, T.E., Woolrich, M.W., Smith, S.M., 2012. Fsl. Neuroimage 62 (2), 782–790.
Jones, D.T., Machulda, M.M., Vemuri, P., McDade, E.M., Zeng, G., Senjem, M.L., Gunter, J.L., Przybelski, S.A., Avula, R.T., Knopman, D.S., Boeve, B.F., Petersen, R.C., Jack, C.R., 2011. Age-related changes in the default mode network are more advanced in Alzheimer disease. Neurology 77 (16), 1524–1531.
Kazemifar, S., Manning, K.Y., Rajakumar, N., Gomez, F.A., Soddu, A., Borrie, M.J., Menon, R.S., Bartha, R., 2017. Spontaneous low frequency BOLD signal variations from resting-state fMRI are decreased in Alzheimer disease. PLoS One 12 (6), e0178529.
Klunk, W.E., Engler, H., Nordberg, A., Wang, Y., Blomqvist, G., Holt, D.P., Bergstrom, M., Savitcheva, I., Huang, G.F., Estrada, S., Ausen, B., Debnath, M.L., Barletta, J., Price, J.C., Sandell, J., Lopresti, B.J., Wall, A., Koivisto, P., Antoni, G., Mathis, C.A., Langstrom, B., 2004. Imaging brain amyloid in Alzheimer's disease with Pittsburgh Compound-B. Ann. Neurol. 55 (3), 306–319.
Laumann, T.O., Gordon, E.M., Adeyemo, B., Snyder, A.Z., Joo, S.J., Chen, M.Y., Gilmore, A.W., McDermott, K.B., Nelson, S.M., Dosenbach, N.U., Schlaggar, B.L., Mumford, J.A., Poldrack, R.A., Petersen, S.E., 2015. Functional system and areal organization of a highly sampled individual human brain. Neuron 87 (3), 657–670.
Laumann, T.O., Snyder, A.Z., Mitra, A., Gordon, E.M., Gratton, C., Adeyemo, B., Gilmore, A.W., Nelson, S.M., Berg, J.J., Greene, D.J., McCarthy, J.E., Tagliazucchi, E., Laufs, H., Schlaggar, B.L., Dosenbach, N.U.F., Petersen, S.E., 2017. On the stability of BOLD fMRI correlations. Cereb. Cortex 27 (10), 4719–4732.
Liang, Y.C., Lee, H.P., Lim, S.P., Lin, W.Z., Lee, K.H., Wu, C.G., 2002. Proper orthognonal decomposition and its applications - part I: theory. J. Sound Vib. 252 (3), 527–544.
Lin, L., Xing, G., Han, Y., 2018. Advances in resting state neuroimaging of mild cognitive impairment. Front. Psychiatry 9, 671.
Luckett, P.H., McCullough, A., Gordon, B.A., Strain, J., Flores, S., Dincer, A., McCarthy, J., Kuffner, T., Stern, A., Meeker, K.L., Berman, S.B., Chhatwal, J.P., Cruchaga, C., Fagan, A.M., Farlow, M.R., Fox, N.C., Jucker, M., Levin, J., Masters, C.L., Mori, H., Noble, J.M., Salloway, S., Schofield, P.R., Brickman, A.M., Brooks, W.S., Cash, D.M., Fulham, M.J., Ghetti, B., Jack, C.R., Voglein, J., Klunk, W., Koeppe, R., Oh, H., Su, Y., Weiner, M., Wang, Q., Swisher, L., Marcus, D., Koudelis, D., Joseph-Mathurin, N., Cash, L., Hornbeck, R., Xiong, C., Perrin, R.J., Karch, C.M., Hassenstab, J., McDade, E., Morris, J.C., Benzinger, T.L.S., Bateman, R.J., Ances, B.M., 2021. Modeling autosomal dominant Alzheimer's disease with machine learning. Alzheimers Dement.
Luo, C., Guo, X., Song, W., Chen, Q., Yang, J., Gong, Q., Shang, H.F., 2015. The trajectory of disturbed resting-state cerebral function in Parkinson's disease at different Hoehn and Yahr stages. Hum. Brain Mapp. 36 (8), 3104–3116.
Madsen, K.H., Churchill, N.W., Morup, M., 2017. Quantifying functional connectivity in multi-subject fMRI data using component models. Hum. Brain Mapp. 38 (2), 882–899.
Marchitelli, R., Aiello, M., Cachia, A., Quarantelli, M., Cavaliere, C., Postiglione, A., Tedeschi, G., Montella, P., Milan, G., Salvatore, M., Salvatore, E., Baron, J.C., Pappata, S., 2018. Simultaneous resting-state FDG-PET/fMRI in Alzheimer Disease: relationship between glucose metabolism and intrinsic activity. Neuroimage 176, 246–258.
Mascali, D., DiNuzzo, M., Gili, T., Moraschi, M., Fratini, M., Maraviglia, B., Serra, L., Bozzali, M., Giove, F., 2015. Intrinsic patterns of coupling between correlation and amplitude of low-frequency fMRI fluctuations are disrupted in degenerative dementia mainly due to functional disconnection. PLoS One 10 (4), e0120988.
Matthews, P.M., Filippini, N., Douaud, G., 2013. Brain structural and functional connectivity and the progression of neuropathology in Alzheimer's disease. J. Alzheimers Dis. 33 (1), S163–S172 Suppl.
McDade, E., Wang, G., Gordon, B.A., Hassenstab, J., Benzinger, T.L.S., Buckles, V., Fagan, A.M., Holtzman, D.M., Cairns, N.J., Goate, A.M., Marcus, D.S., Morris, J.C., Paumier, K., Xiong, C., Allegri, R., Berman, S.B., Klunk, W., Noble, J., Ringman, J., Ghetti, B., Farlow, M., Sperling, R.A., Chhatwal, J., Salloway, S., Graff-Radford, N.R., Schofield, P.R., Masters, C., Rossor, M.N., Fox, N.C., Levin, J., Jucker, M., Bateman, R.J., 2018. Longitudinal cognitive and biomarker changes in dominantly inherited Alzheimer disease. Neurology 91 (14), e1295–e1306.
Mevel, K., Chetelat, G., Eustache, F., Desgranges, B., 2011. The default mode network in healthy aging and Alzheimer's disease. Int. J. Alzheimers Dis. 2011, 535816.
Millar, P.R., Petersen, S.E., Ances, B.M., Gordon, B.A., Benzinger, T.L.S., Morris, J.C., Balota, D.A., 2020. Evaluating the sensitivity of resting-state BOLD variability to age and cognition after controlling for motion and cardiovascular influences: a network-based approach. Cereb. Cortex.
Mishra, S., Gordon, B.A., Su, Y., Christensen, J., Friedrichsen, K., Jackson, K., Hornbeck, R., Balota, D.A., Cairns, N.J., Morris, J.C., Ances, B.M., Benzinger, T.L.S., 2017. AV-1451 PET imaging of tau pathology in preclinical Alzheimer disease: defining a summary measure. Neuroimage 161, 171–178.
Morris, J.C., 1993. The clinical dementia rating (CDR): current version and scoring rules. Neurology 43 (11), 2412–2414.
Ojemann, J.G., Akbudak, E., Snyder, A.Z., McKinstry, R.C., Raichle, M.E., Conturo, T.E., 1997. Anatomic localization and quantitative analysis of gradient refocused echo-planar fMRI susceptibility artifacts. Neuroimage 6 (3), 156–167.
Peng, S.L., Dumas, J.A., Park, D.C., Liu, P., Filbey, F.M., McAdams, C.J., Pinkham, A.E., Adinoff, B., Zhang, R., Lu, H., 2014. Age-related increase of resting metabolic rate in the human brain. Neuroimage 98, 176–183.
Potter, R., Patterson, B.W., Elbert, D.L., Ovod, V., Kasten, T., Sigurdson, W.,

Mawuenyega, K., Blazey, T., Goate, A., Chott, R., Yarasheski, K.E., Holtzman, D.M., Morris, J.C., Benzinger, T.L., Bateman, R.J., 2013. Increased *in vivo* amyloid-beta42 production, exchange, and loss in presenilin mutation carriers. Sci. Transl. Med. 5 (189) 189ra177.

Power, J.D., Barnes, K.A., Snyder, A.Z., Schlaggar, B.L., Petersen, S.E., 2012. Spurious but systematic correlations in functional connectivity MRI networks arise from subject motion. Neuroimage 59 (3), 2142–2154.

Rahim, M., Thirion, B., Varoquaux, G., 2017. Population-Shrinkage of Covariance to Estimate Better Brain Functional Connectivity. Springer International Publishing, Cham.

Raut, R.V., Mitra, A., Snyder, A.Z., Raichle, M.E., 2019. On time delay estimation and sampling error in resting-state fMRI. Neuroimage 194, 211–227.

Resnick, S.M., Pham, D.L., Kraut, M.A., Zonderman, A.B., Davatzikos, C., 2003. Longitudinal magnetic resonance imaging studies of older adults: a shrinking brain. J. Neurosci. 23 (8), 3295–3301.

Ringman, J.M., Monsell, S., Ng, D.W., Zhou, Y., Nguyen, A., Coppola, G., Van Berlo, V., Mendez, M.F., Tung, S., Weintraub, S., Mesulam, M.M., Bigio, E.H., Gitelman, D.R., Fisher-Hubbard, A.O., Albin, R.L., Vinters, H.V., 2016. Neuropathology of autosomal dominant Alzheimer disease in the national Alzheimer coordinating center database. J. Neuropathol. Exp. Neurol. 75 (3), 284–290.

Ripp, I., Stadhouders, T., Savio, A., Goldhardt, O., Cabello, J., Calhoun, V., Riedl, V., Hedderich, D., Diehl-Schmid, J., Grimmer, T., Yakushev, I., 2020. Integrity of neurocognitive networks in dementing disorders as measured with simultaneous PET/functional MRI. J. Nucl. Med. 61 (9), 1341–1347.

Sala-Llonch, R., Bartres-Faz, D., Junque, C., 2015. Reorganization of brain networks in aging: a review of functional connectivity studies. Front. Psychol. 6, 663.

Salat, D.H., Buckner, R.L., Snyder, A.Z., Greve, D.N., Desikan, R.S., Busa, E., Morris, J.C., Dale, A.M., Fischl, B., 2004. Thinning of the cerebral cortex in aging. Cereb. Cortex 14 (7), 721–730.

Scheel, N., Tarumi, T., Tomoto, T., Cullum, C.M., Zhang, R., Zhu, D.C., 2022. Resting-state functional MRI signal fluctuation amplitudes are correlated with brain amyloid-beta deposition in patients with mild cognitive impairment. J. Cereb. Blood Flow Metab. 42 (5), 876–890.

Seitzman, B.A., Gratton, C., Marek, S., Raut, R.V., Dosenbach, N.U.F., Schlaggar, B.L., Petersen, S.E., Greene, D.J., 2020. A set of functionally-defined brain regions with improved representation of the subcortex and cerebellum. Neuroimage 206, 116290.

Sheline, Y.I., Raichle, M.E., 2013. Resting state functional connectivity in preclinical Alzheimer's disease. Biol. Psychiatry 74 (5), 340–347.

Sheline, Y.I., Raichle, M.E., Snyder, A.Z., Morris, J.C., Head, D., Wang, S., Mintun, M.A., 2010. Amyloid plaques disrupt resting state default mode network connectivity in cognitively normal elderly. Biol. Psychiatry 67 (6), 584–587.

Snyder, A.Z., Nishino, T., Shimony, J.S., Lenze, E.J., Wetherell, J.L., Voegtle, M., Miller, J.P., Yingling, M.D., Marcus, D., Gurney, J., Rutlin, J., Scott, D., Eyler, L., Barch, D., 2022. Covariance and correlation analysis of resting state functional magnetic resonance imaging data acquired in a clinical trial of mindfulness-based stress reduction and exercise in older individuals. Front. Neurosci. 16, 825547.

Spreng, R.N., Schacter, D.L., 2012. Default network modulation and large-scale network interactivity in healthy young and old adults. Cereb. Cortex 22 (11), 2610–2621.

Su, Y., D'Angelo, G.M., Vlassenko, A.G., Zhou, G., Snyder, A.Z., Marcus, D.S., Blazey, T.M., Christensen, J.J., Vora, S., Morris, J.C., Mintun, M.A., Benzinger, T.L., 2013. Quantitative analysis of PiB-PET with FreeSurfer ROIs. PLoS One 8 (11), e73377.

Teipel, S.J., Bokde, A.L., Meindl, T., Amaro Jr., E., Soldner, J., Reiser, M.F., Herpertz, S.C., Moller, H.J., Hampel, H., 2010. White matter microstructure underlying default mode network connectivity in the human brain. Neuroimage 49 (3), 2021–2032.

Tentolouris-Piperas, V., Ryan, N.S., Thomas, D.L., Kinnunen, K.M., 2017. Brain imaging evidence of early involvement of subcortical regions in familial and sporadic Alzheimer's disease. Brain Res. 1655, 23–32.

Thomas, J.B., Brier, M.R., Bateman, R.J., Snyder, A.Z., Benzinger, T.L., Xiong, C., Raichle, M., Holtzman, D.M., Sperling, R.A., Mayeux, R., Ghetti, B., Ringman, J.M., Salloway, S., McDade, E., Rossor, M.N., Ourselin, S., Schofield, P.R., Masters, C.L., Martins, R.N., Weiner, M.W., Thompson, P.M., Fox, N.C., Koeppe, R.A., Jack, C.R., Mathis, C.A., Oliver, A., Blazey, T.M., Moulder, K., Buckles, V., Hornbeck, R., Chhatwal, J., Schultz, A.P., Goate, A.M., Fagan, A.M., Cairns, N.J., Marcus, D.S., Morris, J.C., Ances, B.M., 2014. Functional connectivity in autosomal dominant and late-onset Alzheimer disease. JAMA Neurol. 71 (9), 1111–1122.

Toepper, M., 2017. Dissociating normal aging from Alzheimer's disease: a view from cognitive neuroscience. J. Alzheimers Dis. 57 (2), 331–352.

Varoquaux, G., Gramfort, A., Poline, J.B., Thirion, B., Lafferty, J.D., Williams, C.K.I., Shawe-Taylor, J., Zemel, R.S., Culotta, A., 2010. Brain covariance selection: better individual functional connectivity models using population prior. In: Advances in Neural Information Processing Systems 23. Curran Associates, Inc., pp. 2334–2342.

Vieira, B.H., Rondinoni, C., Garrido Salmon, C.E., 2020. Evidence of regional associations between age-related inter-individual differences in resting-state functional connectivity and cortical thinning revealed through a multi-level analysis. Neuroimage 211, 116662.

Wang, J., Sun, H., Cui, B., Yang, H., Shan, Y., Dong, C., Zang, Y., Lu, J., 2021. The relationship among glucose metabolism, cerebral blood flow, and functional activity: a Hybrid PET/fMRI study. Mol. Neurobiol. 58 (6), 2862–2873.

Wang, L., Roe, C.M., Snyder, A.Z., Brier, M.R., Thomas, J.B., Xiong, C., Benzinger, T.L., Morris, J.C., Ances, B.M., 2012. Alzheimer disease family history impacts resting state functional connectivity. Ann. Neurol. 72 (4), 571–577.

White, R.L., Campbell, M.C., Yang, D., Shannon, W., Snyder, A.Z., Perlmutter, J.S., 2020. Little change in functional brain networks following acute levodopa in drug-naive parkinson's disease. Mov. Disord. 35 (3), 499–503.

Wong, D.F., Rosenberg, P.B., Zhou, Y., Kumar, A., Raymont, V., Ravert, H.T., Dannals, R.F., Nandi, A., Brasic, J.R., Ye, W., Hilton, J., Lyketsos, C., Kung, H.F., Joshi, A.D., Skovronsky, D.M., Pontecorvo, M.J., 2010. *In vivo* imaging of amyloid deposition in Alzheimer disease using the radioligand 18F-AV-45 (florbetapir [corrected] F 18). J. Nucl. Med. 51 (6), 913–920.

Yang, L., Yan, Y., Wang, Y., Hu, X., Lu, J., Chan, P., Yan, T., Han, Y., 2018. Gradual disturbances of the amplitude of low-frequency fluctuations (ALFF) and fractional ALFF in Alzheimer spectrum. Front. Neurosci. 12, 975.

Zeng, Q., Luo, X., Li, K., Wang, S., Zhang, R., Hong, H., Huang, P., Jiaerken, Y., Xu, X., Xu, J., Wang, C., Zhou, J., Zhang, M., 2019. Distinct spontaneous brain activity patterns in different biologically-defined Alzheimer's disease cognitive stage: a preliminary study. Front. Aging Neurosci. 11, 350.

Zhang, J., Kucyi, A., Raya, J., Nielsen, A.N., Nomi, J.S., Damoiseaux, J.S., Greene, D.J., Horovitz, S.G., Uddin, L.Q., Whitfield-Gabrieli, S., 2021. What have we really learned from functional connectivity in clinical populations? Neuroimage 242, 118466.

Zhang, Y., Brady, M., Smith, S., 2001. Segmentation of brain MR images through a hidden Markov random field model and the expectation-maximization algorithm. IEEE Trans. Med. Imaging 20 (1), 45–57.

Zuo, X.N., Di Martino, A., Kelly, C., Shehzad, Z.E., Gee, D.G., Klein, D.F., Castellanos, F.X., Biswal, B.B., Milham, M.P., 2010. The oscillating brain: complex and reliable. Neuroimage 49 (2), 1432–1445.